AIMS Mathematics, 10(6): 14804–14839.
DOI: 10.3934/math.2025666
Received: 26 April 2025
Revised: 02 June 2025
Accepted: 16 June 2025
Published: 27 June 2025

http://www.aimspress.com/journal/Math

Research article

Exploring assisting and opposing flow characteristics in a saturated darcy medium with non-uniform heat source or sink and suspended microbes

Khalid Masood*

Department of Mathematics and Statistics, College of Science, Imam Mohammad Ibn Saud Islamic University (IMSIU), Riyadh 11623, Saudi Arabia

* **Correspondence:** Email: kmaali@imamu.edu.sa.

Abstract: Aim of the study: In this study, I investigated buoyancy-driven convection involving suspended microorganisms in a saturated Darcy porous medium, considering the effects of thermal radiation, Brownian motion, thermophoresis, and non-uniform heat source/sink. I focused on slender geometries, specifically a cone and a cylinder, under both assisting and opposing flow conditions, to better understand their impact on heat and mass transfer behavior. **Significance and novelty:** Bio-convection has wide-ranging applications in drug delivery, cancer therapy, electronics cooling, microbial fuel cells, water purification, and cosmetic formulations. Unlike other researchers, I uniquely integrated the effects of non-uniform thermal conditions, gyrotactic microorganism dynamics, and slender body geometry. The inclusion of a multilinear regression model added an analytical layer for interpreting parameter sensitivity, which enhanced the model's utility in engineering design. **Methodology:** The governing nonlinear partial differential equations were transformed into a system of ordinary differential equations using similarity transformations. These equations were solved numerically using the fourth-order Runge-Kutta method coupled with a shooting technique. To further analyze parametric trends, multilinear regression was applied to the simulation data. **Results and insights:** The presence of gyrotactic microorganisms significantly enhanced mass transfer rates compared to microbe-free scenarios. An increase in thermophoresis led to higher temperature distributions but reduced both concentration and microorganism density. Fluid velocity increased under assisting flows due to stronger buoyancy forces. These trends were demonstrated through detailed stream function and temperature plots and numerical findings for important flow and heat transfer parameters in tabular form for the flow dynamics. **Conclusion:** This study provides

meaningful insights into the role of microorganisms in enhancing mass and heat transfer in porous media. The model serves as a strong foundation for future extensions involving experimental validation, time-dependent simulations, turbulent bio-convection, and more complex geometrical configurations for industrial and biomedical applications.

Keywords: micro-organisms; multi-linear regression (MLR); non-uniform heat source or sink; Thermal radiation; porous channel; buoyancy; slender body of revolution

Nomenclature:

u, v	Velocity components	$A, B, C,$ a, b, c	Constant in equation (7)
T	Nanofluid temperature	$\widehat{\psi}$	Stream function
T_∞	Ambient temperature	f	Dimensionless stream function
T_w	Surface temperature	α	Thermal diffusivity of the porous medium
C	Nanoparticles concentration	D_B	Brownian coefficient
β_T	Coefficient of thermal expansion	Nc	Buoyancy ratio
β_c	Coefficient of concentration expansion	Nr	Thermal radiation parameter
τ	Volumetric heat capacity	Le	Lewis number
ρc_p	Heat capacity	Pe	Peclet number
q_r	Radiative heat flux	Nb	Brownian Parameter
K	Thermal conductivity	Nt	thermophoresis parameter
D_T	Coefficient of thermophoresis diffusion	Nu	Nusselt Number
N	Micro-organism	Sh	Sherwood number
ξ	Independent similarity variable	NSh	Diffusivity of micro-organism
θ	Dimensionless temperature	k^+	represent the mean absorption
ϕ	Dimensionless concentration	γ^+	the Stefan Boltzmann constant
χ	Dimensionless micro-organism	$\widehat{\psi}$	Stream function
$A^* > 0, B^* > 0$	signifies heat generation	$A^* < 0, B^* < 0$	heat absorption

1. Introduction

Microorganisms, encompassing bacteria, archaea, and fungi, wield significant influence in fluid mechanics and thermal engineering. In fluid dynamics, microorganisms contribute to biofilm formation, affecting friction and pressure drop in industrial pipelines. Biofouling, the accumulation of microorganisms on submerged surfaces, poses challenges but also sparks research into biofouling

control methods. In thermal engineering, microbial fuel cells leverage bacterial metabolism to convert organic matter into electrical energy, holding promise for applications in wastewater treatment and organic-rich effluents. Extremophiles, adapted to extreme conditions, are explored for their potential in geothermal energy extraction and acidic waste treatment. Additionally, microorganisms enhance heat transfer efficiency, with bioaugmentation employing specific bacteria to optimize organic waste treatment and increase biogas production. The diverse applications underscore the pivotal role microorganisms play in shaping fluid dynamics and thermal processes across industries, offering sustainable solutions and innovative avenues for energy production and waste management. Extensive research on nanofluids incorporating both gyrotactic microorganisms and nanoparticles, like algae, has been limited until now. Pioneering studies by the researchers in [1–5] extensively explored bioconvection phenomena in suspensions containing solid particles. Rao et al. [6] studied the bioconvection induced by suspended gyrotactic bacteria above a thermally heated surface, while the researchers [7–9] examined the effect of oxytactic bacteria moving upward on heat convection. The integration of gyrotactic microbes into nanofluids is anticipated to improve suspension equilibrium, as these microorganisms have demonstrated a propensity toward bioconvection, leading to macroscopic fluid motion [10–12]. Analytical solutions, as presented in [13], addressed the flow of a rotating fluid on a rotating cone using magnetohydrodynamics (MHD). Subsequently, in [14], an analysis was conducted on free convection in nanofluids near a permeable horizontal circular cylinder, revealing that increased suction significantly enhances the concentration of motile microorganisms. This density increase is attributed to swimming motion that is upward induced by stimuli like chemical attractions, light, and gravity, generating unstable density stratification and fostering hydrodynamic uncertainty. Further investigations, including [15], where researchers investigated gyrotactic microorganisms in a nanofluid undergoing stagnation flow over a stretched sheet, and [16], where researchers focused on examining the mass and heat transfer characteristics of MHD bioconvection within dual-channel configurations, illuminate the complex interactions that occur between various flow geometries, magnetic fields, nanofluids and microbes. These studies provide valuable insights into the complex dynamics of fluids under the influence of various factors.

Slender bodies are geometric shapes characterized by a long length compared to their cross-sectional dimensions, and they play a crucial role in fluid mechanics and thermal engineering. Common types include cylinders, cones, and airfoils, each exhibiting unique flow characteristics. In fluid mechanics, the slender body theory simplifies the analysis of streamlined structures, enabling accurate predictions of flow patterns without the complexity of three-dimensional effects. This theory is especially valuable in aerodynamics for understanding the behavior of aircraft wings, missiles, and other streamlined objects. In thermal engineering, slender bodies are integral to heat exchanger design, where their streamlined shapes reduce drag and enhance heat transfer efficiency. Moreover, in applications like electronics cooling, slender bodies aid in managing airflow to optimize thermal performance. The study and application of slender bodies contribute significantly to the advancement of fluid dynamics and heat transfer in diverse engineering fields. The study outlined in [17] draws attention to the fact that Lewis numbers have a greater impact on concentration fields than on flow or temperature. Investigations into the flux of heat from the outer surfaces of hot bodies in saturated porous media, as discussed in [18], bear substantial implications in engineering and geophysics. Earlier studies, referenced in [19], mostly entailed fundamental geometries, such as cylinders or flat plates, leading to the analytical equation's derivation related to boundary layer thickness, local and overall heat flux over the surface, and heat transfer coefficients at each scale. Notably, the researchers in [20]

explored the impact of different physical parameters on velocity and concentration velocity characteristics of wall thermophoretic deposition. The researchers in [21] demonstrated that, as the axial length increases along the cylinder, forced convection increasingly dominates the heat transfer process. In a related study, the researchers in [22] examined thermal analysis of slender rotational bodies, taking into account free and mixed convection through a saturated porous medium. It was observed that a smaller dimensional radius led to a lower Nusselt number. Additionally, [23] contributed valuable insights into heat transfer behavior in porous media by simultaneously examining heat and mass transfer from slender rotating bodies in saturated porous media. Trihybrid (Co+ZrO2+Au/H2O) nanofluid flow through an exponentially deformable surface with Lorentz force and Navier's slippage constraint was studied thermally by Hussain et al. [24], while Alraddadi et al. [25] looked into the effects of aligned Lorentz force and slippage constraint on ternary hybrid nanofluid flow over an exponentially deformable surface. Mabrouk et al. [26] examined enhanced Bioconvection Adjacent to Permeable Cylinder in Hybrid Nanofluids: Bacteria Distribution and Physical Features under Magnetic Field Influence, and Ahmed et al. [27] examined the use of ternary hybrid nanoparticles to investigate the bioconvective flow surrounding a thin surgical needle in blood. Ternary hybrid nanoparticles, which contain three different nanoparticles in one system, are now widely seen as promising for thermal enhancement. The combination of the special nanoparticle properties allows ternary hybrids to greatly increase thermal conductivity, transfer more heat and provide better stability. They are particularly useful for better managing heat in heat exchangers, cooling systems and storage devices which need smooth and strong thermal management. It has been observed that the correct choice of nanoparticles, their shapes and the amounts used in ternary hybrid systems, can get past the barriers of individual or dual nanoparticles, making way for future innovations in thermal technology (some recent results are [28–30]).

Research gap and novel contributions of this study:

In response to the stated research objective, a detailed investigation was carried out to examine natural convection in radiative flow over slender bodies, accounting for the presence of microorganisms and the influence of a non-uniform heat source or sink. Numerical computations were conducted using the shooting method to achieve the required level of accuracy. By systematically varying the relevant parameters, the results were illustrated through graphical representations. Our central focus of this study was to analyze the following key research questions:

Considering the limited contribution of energy flux from thermal radiation and natural buoyancy due to temperature differences, what is the resulting influence of increased non-uniform heat source/sink intensity and flow direction (assisting or opposing) on heat and mass transfer rates, including the Sherwood number for microorganisms, in flows over slender bodies?

1) How do changes in non-uniform heat source/sink and thermal radiation at different phases influence the transport phenomena of energy, momentum, and micro-organisms within the framework of assisting and opposing flows via slender bodies of revolution?
2) Is it possible for multiple regression analysis to accurately forecast how various elements will affect the system's non-linear dynamics?

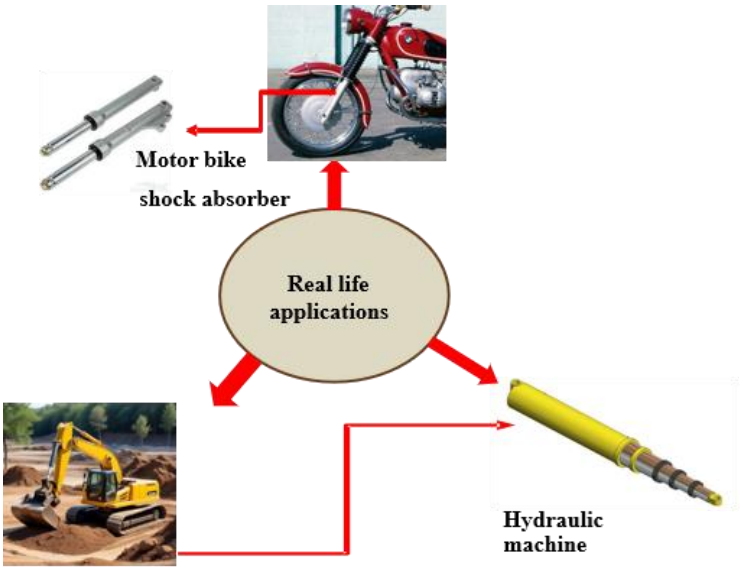

Figure 1. Real life applications of assisting and opposing flow.

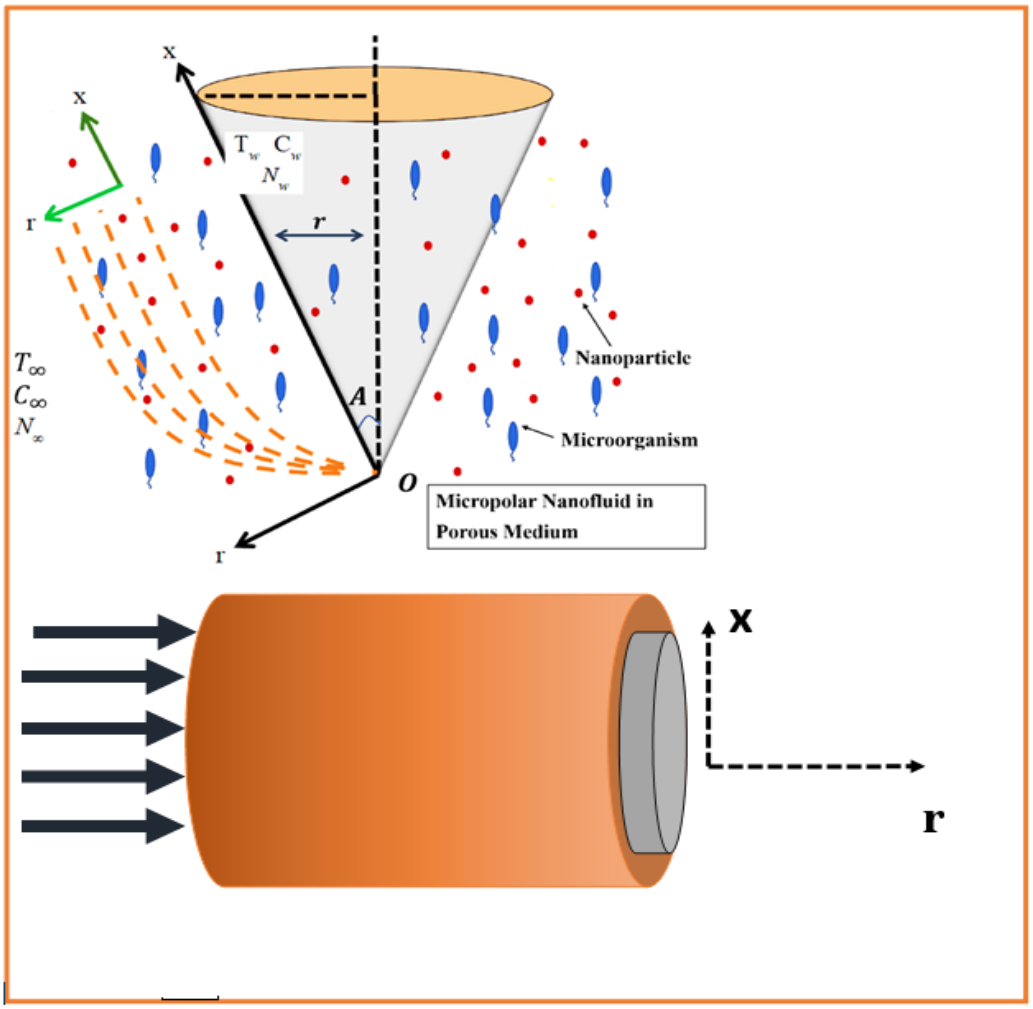

Figure 2. Schematic diagram of flow model.

2. Mathematical formulation

Conducted an analysis of the buoyancy effects, considering both thermal and diffusion aspects, on a slender revolution form situated in a waterlogged porous medium with heat generation or absorption. The impact of thermal radiation is assessed to enhance transport phenomena. Under these circumstances, the surface temperature T_w rises above the far-field temperature T_∞. The cylindrical structure (x,r) represents the coordinate distance along different slender revolutions and perpendicular to the revolving slender surface, with the body vertex at the origin. Figure 1 illustrates the flow structure. The major equations describing the observed flow are described in detail (Raju et al. [31,32] and Bharat Kumar et al. [33]), combining with Boussinesq approximations (BA), thermophoretic effects, Brownian motion, and Darcy saturated porous media with thermal radiation properties.

$$\frac{\partial(ru)}{\partial x}+\frac{\partial(rv)}{\partial r}=0, \tag{1}$$

$$\frac{1}{r}\frac{\partial\bar{\Psi}}{\partial r}=\left(\frac{Kg}{\upsilon}\right)\left[-\beta_T\left(T_\infty-T\right)-\beta_c\left(C_\infty-C\right)\right], \tag{2}$$

$$\frac{\partial\bar{\Psi}}{\partial r}\frac{\partial T}{\partial x}-\frac{\partial\bar{\Psi}}{\partial x}\frac{\partial T}{\partial r}=(\alpha)\frac{\partial}{\partial r}\left(r\frac{\partial T}{\partial r}\right)+(r\tau)\left(D_B\frac{\partial T}{\partial r}\frac{\partial C}{\partial r}+\frac{D_T}{T_\infty}\left(\frac{\partial T}{\partial r}\right)^2\right)\pm\frac{q'''}{\rho c_p}-\frac{1}{\rho c_p}\frac{\partial}{\partial r}(rq_r), \tag{3}$$

$$\frac{\partial\bar{\Psi}}{\partial r}\frac{\partial C}{\partial x}-\frac{\partial\bar{\Psi}}{\partial x}\frac{\partial C}{\partial r}=(D_B)\frac{\partial}{\partial r}\left(r\frac{\partial C}{\partial r}\right)+\left(\frac{D_T}{T_\infty}\right)\frac{\partial}{\partial r}\left(r\frac{\partial T}{\partial r}\right), \tag{4}$$

$$\frac{\partial\bar{\Psi}}{\partial r}\frac{\partial N}{\partial x}-\frac{\partial\bar{\Psi}}{\partial x}\frac{\partial N}{\partial r}+\frac{bw_c}{C_\infty}\left[\frac{\partial}{\partial r}\left(N\frac{\partial C}{\partial r}\right)\right]=D_n\frac{\partial}{\partial r}\left(r\frac{\partial N}{\partial r}\right). \tag{5}$$

The Boussinesq approximations are used by.

$$\left(\frac{\rho}{\rho_\infty}\right)=(-1)\left[-1+\beta_T\left(T-T_\infty\right)+\beta_c\left(C-C_\infty\right)\right]. \tag{6}$$

The boundary conditions are:

$$\text{At, } r=R(x)$$

$$v=0,\quad T=T_w(x)-T_\infty=Ax^{(a)}\ ,C=C_w(x)-C_\infty=Bx^{(b)}\ ,N=N_w(x)-N_\infty=Nx^{(c)}. \tag{7}$$

At infinity,

$$u(r\to\infty)=0,\quad C(r\to\infty)=C_\infty,\ T(r\to\infty)=T_\infty,\ \ N(r\to\infty)=N_\infty. \tag{8}$$

The evaluation of thermal radiation [24,25]

$$q_r = -\frac{4\gamma^+}{3k^+}\left(\frac{\partial T^4}{\partial r}\right). \tag{9}$$

Expanding the fourth power of temperature T^4 through a Taylor series with respect to temperature and excluding terms involving complex orders produces the ensuing outcome.

$$T^{(4)} \cong (4)T_\infty^{(3)}T - 3T_\infty^{(4)}. \tag{10}$$

By substituting Eq (10) into Eq (9), and incorporating the result into Eq (3), the final expression is obtained.

$$\frac{\partial\widehat{\Psi}}{\partial r}\frac{\partial T}{\partial x} - \frac{\partial\widehat{\Psi}}{\partial x}\frac{\partial T}{\partial r} = \alpha\left(1+\frac{4}{3}N_r\right)\frac{\partial}{\partial r}\left(r\frac{\partial T}{\partial r}\right) + r\tau\left(D_B\frac{\partial T}{\partial r}\frac{\partial C}{\partial r} + \frac{D_T}{T_\infty}\left(\frac{\partial T}{\partial r}\right)^2\right) \pm \frac{1}{\rho c_p}q'''. \tag{11}$$

Here, $Nr = \dfrac{4\gamma^+ T_\infty^{(3)}}{kk^+}$ is the thermal radiation.

q''' is defined as the fluid's non-uniform heat source/sink (Bharat Kumar et al. [25]),

$$q''' = \frac{rRa}{x^2}\left[A^*\left(T_w - T_\infty\right)f' + B^*\left(T - T_\infty\right)\right]. \tag{12}$$

Here, when $A^* > 0$ and $B^* > 0$, it denotes a heat source, and when $A^* < 0$ and $B^* < 0$, it signifies an internal heat sink. Here, A^* and B^* represent the temperature-dependent parameters for the heat source/sink, with A^* being positive for heat and negative for a heat sink.

Dimensionless functions and the similarity variable's expression $f(\xi), \theta(\xi), \phi(\xi)$ and $\chi(\xi)$ are defined as

$$\left\{\begin{array}{ll} \xi = Ra\left(\dfrac{r}{x}\right)^2, Ra = \dfrac{Kg\beta_T\left(T_w - T_\infty\right)x}{\alpha\upsilon}, & u = \left(\dfrac{1}{r}\right)\partial\widehat{\Psi}/\partial r, \quad v = \left(-\dfrac{1}{r}\right)\partial\widehat{\Psi}/\partial x \\ \widehat{\Psi} = (\alpha x)f(\xi), & T - T_\infty = \left(T_w - T_\infty\right)\left(\theta(\xi)\right), \\ C - C_\infty = \left(C_w - C_\infty\right)\left(\phi(\xi)\right), & N - N_\infty = \left(N_w - N_\infty\right)\left(\chi(\xi)\right), \end{array}\right\}. \tag{13}$$

Here, the stream function is $\widehat{\Psi}$, Ra -modified local Rayleigh number. Considering $\xi = \xi_0$ (ξ_0 the fixed constant), which signifies a mathematically small value for the revolution of the body, Eq (11) for the slender revolution is expected to account for both its size and shape.

$$R(x)=\left(\frac{\upsilon\alpha\xi_0}{Kg\beta_T A}\right)^{0.5} x^{\left(\frac{1-a}{2}\right)}. \tag{14}$$

In applied situations, parameter ' a ' must satisfy the condition $a\le 1$ to maintain real-world application. For example, a revolution that produces a cylinder of revolution related to $a=0$, while revolution that produces a cone form corresponds to $a=-1$.

After the transition, the governing structure is as follows.

$$f'(\xi)=\tfrac{1}{2}\left(\theta(\xi)+Nc\phi(\xi)\right), \tag{15}$$

$$\left(1+\tfrac{4}{3}Nr\right)\theta''(\xi)=\tfrac{1}{2}\xi\begin{pmatrix} af'(\xi)\theta(\xi)-f(\xi)\theta'(\xi)- \\ 2\theta'(\xi)-\frac{1}{2}\left(A^* f'+B^*\theta\right)\end{pmatrix}-\begin{pmatrix} Nb\theta'(\xi)\phi'(\xi) \\ +Nt\theta'(\xi)^2\end{pmatrix}, \tag{16}$$

$$\phi''(\xi)=\tfrac{1}{2}\xi\left(bLef'(\xi)\phi(\xi)-Lef(\xi)\phi'(\xi)-2\phi'(\xi)-\tfrac{2}{Le}\left(\frac{Nt}{Nb}\right)\left(\theta'(\xi)+\theta''(\xi)\right)\right), \tag{17}$$

$$\chi''(\xi)=\tfrac{1}{2}\xi\left(cLef'(\xi)\chi(\xi)-Lef(\xi)\chi'(\xi)+pe\begin{pmatrix}\chi(\xi)\phi'(\xi)+2\phi\chi'\xi \\ +2\chi(\xi)\phi''(\xi)\xi\end{pmatrix}-2\chi'(\xi)\right). \tag{18}$$

The modified boundary conditions are:

$$\xi=\xi_0,\quad f(\xi)+(a_1-1)\xi f'(\xi)=0,\quad \theta(\xi)=1,\quad \phi(\xi)=1\quad \chi(\xi)=1, \tag{19}$$

$$\xi\to\infty,\quad f'(\xi)=0,\quad \theta(\xi)=0,\quad \phi(\xi)=0\quad \chi(\xi)=0. \tag{20}$$

Here, $Nc=\dfrac{\beta_{c1}(C_w-C_\infty)}{\beta_{T1}(T_w-T_\infty)}$ the ratio of buoyancy, $Nb=\dfrac{(C_w-C_\infty)D_B\tau}{\alpha}$ the Brownian parameter, $Nt=\dfrac{(T_w-T_\infty)D_T\tau}{T_\infty\alpha}$ thermophoresis constant, $Le=\dfrac{\alpha}{D_B}$ Lewis number. $pe=\dfrac{bw_c}{D_n}$ Peclet number.

Equations (15) to (20) in this study provide the framework for two separate numerical solutions:

1) When both a and b are set to 0, the system depicts fluid flow with a cylinder of revolution.

2) When both a and b are set to 1, the system symbolizes a cone of revolution-shaped fluid flow.

The constants linked with both diffusion and thermal transmission are of great interest in practical situations and are described as follows.

$$Nu=\frac{hx}{k}=-\frac{\partial T/\partial r\big|_{r=R(x)}}{T_w-T_\infty}=-2\xi_0^{0.5}Ra^{0.5}\theta'(\xi_0), \tag{21}$$

$$Sh = \frac{mx}{D_B\left(C_w - C_\infty\right)} = -2\xi_0^{0.5} Ra^{0.5} \phi'\left(\xi_0\right), \tag{22}$$

$$NSh = \frac{mx}{D_B\left(N_w - N_\infty\right)} = -2\xi_0^{0.5} Ra^{0.5} \chi'\left(\xi_0\right). \tag{23}$$

2.1. Numerical scheme

The methodological framework for this study is adapted from the work of Hussain et al. [34]. Specifically, Eqs (15–18) are employed under the boundary conditions defined in Eqs (19–20) to model the fluid flow of microorganisms within a porous channel. Due to the complexity and nonlinearity of the governing equations, obtaining an exact analytical solution is challenging. Therefore, a numerical solution is sought using a boundary value problem approach. To this end, the shooting method combined with the classical Runge-Kutta technique is applied. The Runge-Kutta method, widely recognized for its accuracy and efficiency, is a family of iterative procedures designed to approximate the solutions of ordinary differential equations (ODEs). In this context, I begin by addressing the problem as an initial value problem (IVP) before proceeding with the boundary value solution.

$$\frac{dz}{dt} = f(t, z(t)),$$

$$z(t) = (z_1(t), z_2(t), z_3(t), \ldots z_n(t))^T, \quad f \in [a,b] \times R^n \to R^n.$$

With initial conditions $z(0) = z_0$.

The continuously differentiable solution $z(t)$ of the IVP over a specified time interval $t \in [a,b]$ is of particular interest for numerical approximation. To facilitate this, the interval is partitioned into equal subintervals $[a,b]$ by selecting appropriate mesh points M. The length of each subinterval is referred to as the step size, denoted by h. The class of explicit Runge-Kutta (RK) methods with m^{th} stages can then be formulated accordingly.

$$\mathrm{Z}(\tilde{t}_n + 1) = \mathrm{Z}_n + 1 = \mathrm{Z}_n + h\sum_{i=1}^{m} c_i \tilde{L}_i.$$

Here,

$$\tilde{L}_1 = f(\tilde{t}_n + \mathrm{Z}_n),$$

$$\tilde{L}_2 = f\left(\tilde{t}_n + a_2 h, \quad \mathrm{Z}_n + h\beta_{21}\tilde{L}_1(\tilde{t}_n + \mathrm{Z}_n)\right),$$

$$\tilde{L}_3 = f\left(\tilde{t}_n + a_{3h,} \ \mathrm{Z}_n + h\left(\beta_{31}\tilde{L}_1(\tilde{t}_n + \mathrm{Z}_n) + \beta_{32}\tilde{L}_2(\tilde{t}_n + \mathrm{Z}_n)\right)\right),$$

$$\tilde{L}_m = f\left(\tilde{t}_n + a_m h,\ \mathrm{Z}_n + h\sum_{i=1}^{m-1}\beta m_j \tilde{L}_j)\right).$$

To apply this method, the higher-order derivatives in Eqs (14–19) must first be transformed into an equivalent system of first-order differential equations, as demonstrated below:

$$f = f_1,\quad \theta = f_2,\quad \theta' = f_3,\quad \phi = f_4,\quad \phi' = f_5,\quad \chi = f_6,\quad \chi' = f_7,$$

$$f = f_1\quad ,$$

$$f_1^{'} = \tfrac{1}{2}\left(\theta(\xi) + Nc\phi(\xi)\right)\ ,$$

$$f_3^{'} = \frac{\tfrac{1}{2}\xi\begin{pmatrix} af'(\xi)\theta(\xi) - \\ f(\xi)\theta'(\xi) - 2\theta'(\xi)\end{pmatrix} - \begin{pmatrix} Nb\theta'(\xi)\phi'(\xi) \\ +Nt\theta'(\xi)^2\end{pmatrix}}{\left(1+\tfrac{4}{3}Nr\right)},$$

$$f_4^{'} = f_5,$$

$$f_5^{'} = \tfrac{1}{2}\xi\left(bLef'(\xi)\phi(\xi) - Lef(\xi)\phi'(\xi) - 2\phi'(\xi) - \tfrac{2}{Le}\left(\frac{Nt}{Nb}\right)\left(\theta'(\xi) + \theta''(\xi)\right)\right),$$

$$f_6^{'} = f_7,$$

$$f_7^{'} = \tfrac{1}{2}\xi\left(cLef'(\xi)\chi(\xi) - Lef(\xi)\chi'(\xi) + pe\begin{pmatrix}\chi(\xi)\phi'(\xi) + 2\phi\chi'\xi \\ +2\chi(\xi)\phi''(\xi)\xi\end{pmatrix} - 2\chi'(\xi)\right),$$

With boundary conditions

$$fa(1) + (a-1)\xi(0.5(fa(2) + Nc * fa(4)))\,,\ fa(2) - 1,\ fa(4) - 1,\ fa(6) - 1,$$

$$fb(2) - 1,\ fb(4) - 1, fb(6) - 1.$$

2.2. *Multilinear statics of regression (MLR)*

Within the regression model, $\mathbb{R} = A_1X_1 + A_2X_2 + B..., A_1, A_2...$ the slopes correspond to the regression coefficient, $X_1, X_2...$ are treated as independent parameter. Multilinear regression equation for the Nusselt number, Sherwood number and Micro-organism Sherwood number are.

For Nusselt numbers (Nus)

$$Nus1 = -0.302814832793959 * Nr - 0.128630636461704 * Le + 0 * Pe -$$
$$-0.288232783171521 * Nb + 0 * Nt + 0 * A + 0.206577961165049 * B + 1.4027205188781\,'$$

$$Nus2 = -14.2126850636462*Nr+18.5221234358144*Le+0*Pe- \\ -8.84641158576054*Nb+0*Nt+0*A+71.2100905825243*B+1.86937810571737,$$

$$Nus3 = -0.299291430420712*Nr-0.157302103559871*Le+0*Pe- \\ -0.228979029126213Nb+0*Nt+0*A+0.185086990291262*B+1.36749693527508,$$

$$Nus4 = -2.45927971521036*Nr+2.80160394822006*Le+0*Pe- \\ -1.57003951456311*Nb+0*Nt+0*A+11.3125534951456+1.36358396763754.$$

For Sherwood numbers (Shr)

$$Shr1 = 2.92751370658037*Nr+3.38913956850054*Le+0*Pe- \\ -2.77902595469256*Nb+0*Nt+0*A-2.33324087378641*B-0.0216569363538266,$$

$$Shr2 = 46.4017732556634*Nr-52.3148016828479*Le+0*Pe+ \\ +22.5601307766991*Nb+0*Nt+0*A-222.564996407767*B-1.87644805177992,$$

$$Shr3 = 3.11475228910464*Nr+4.23518718985976*Le+0*Pe- \\ -3.37502177993527*Nb+0*Nt+0*A-3.29014281553398*B+0.173818451995685,$$

$$Shr4 = 11.6892485717368*Nr-6.46013798274003*Le+0*Pe+ \\ +1.5104798381877*Nb+0*Nt+0*A-46.8852211650485*B-0.129436322545843.$$

For Micro-organisms Sherwood number (NShr)

$$NShr1 = 0.00732170442286928*Nr+2.62770544768069*Le+0*Pe+ \\ +1.79911517799353*Nb+0*Nt+0*A-3.8367127184466*B+3.3544983214671,$$

$$NShr2 = 18.9647497626753*Nr-21.1621032901834*Le+0*Pe+ \\ +12.8274145954693*Nb+0*Nt+0*A-100.061952912621*B+2.34536236030205,$$

$$NShr3 = 2.87230812513484*Nr+2.56017900755124*Le+0*Pe- \\ -2.21727569579288*Nb+0*Nt+0*A-0.010113009708737*B-0.0164689536138067,$$

$$NShr4 = 5.05403643365696*Nr+0.314603284789641*Le+0*Pe- \\ -1.18555766990291*Nb+0*Nt+0*A-10.697119223301*B-0.297788822006471.$$

3. Results and discussion

The system of ordinary differential equations (ODEs) represented by (15), (16), (17), and (18) under the specified conditions [Eqs (19) and (20)] is analyzed mathematically by employing the Runge-Kutta approach. For accurate numerical results, essential parameters such as $Nt=0.4, Nb=0.4, B^*=0.5, A^*=0.5, Nr=01, Le=0.5,\ Pe=0.5, n=0.5$ are considered, and I have set the value of $Nc=0.5$ for assisting flow and $Nc=-0.0023$ for opposing flow in both cone and

cylinder cases. These standards are consistently maintained throughout the entire investigation, excluding variances presented in the relevant tables and graphs. When depicted graphically, solid lines (green and yellow) represent fluid in assisting flow, whereas dashed lines (blue and red) denote fluid in opposing flow.

The effects of (Nt) on the micro-organisms field, velocity, concentration, and temperature are depicted in Figures 3, 4, 5, and 6, respectively. With rising values of (Nt) both concentration and the micro-organisms field declines, while velocity and temperature fields boost for both opposing and assisting flows in both revolution shapes (cone and cylinder). Elevated values of the Thermophoresis diffusion coefficient result in increased fluid velocity due to changes in the Thermophoretic force acting on fluid particles, potentially altering temperature gradients and causing an elevation in the temperature field.

The influence of the Peclet number (Pe) on the micro-organisms field, concentration, velocity, and temperature is illustrated in Figures 7–10. With the enhancement in (Pe), the concentration and micro-organisms field drops, while temperature and velocity grows in both cases (cone and cylinder) and for both flow directions (assisting and opposing). This occurs as a result of the increased in (Pe) implies stronger advection relative to diffusion, leading to faster fluid flow and influencing the overall velocity field.

The influence of non-uniform heat generation (A^*) on micro-organisms profiles, temperature, concentration, and velocity fields is portrayed in Figures 11–14. With intensified values of the non-uniform heat generation parameter, temperature and velocity fields expand, while concentration and the micro-organisms field decline in both situations (assisting and opposing flows in cone and cylinder). Physically, higher values of heat generation induce convective currents, potentially increasing fluid velocity and temperature.

The effect of non-uniform heat absorption (B^*) on micro-organisms profiles, temperature, concentration, and velocity fields is depicted in Figures 15–18. When the values of the non-uniform heat absorption parameter rise, the fluid velocity increases while temperature, concentration, and the micro-organisms field decrease in both cases (assisting and opposing flows in cone and cylinder). Physically, increased non-uniform heat absorption extracts energy from the fluid, reducing temperature, concentration, and microorganism activity.

With the increment of (Nr), the fluid velocity has increased and a decrement in micro-organisms profiles in both cases (assisting flow and opposing flow), as observed in Figures 19 and 20. In practice, (Nr) is a measure of the ratio of conduction heat transport to energy transmission, so higher values of (Nr) advocate for more control of heat transfer via conduction. Applications such as solar collectors, biomedical heating, and high-temperature porous insulation systems have radiative effects that

dominate heat transport.

The impact of the Lewis number (Le) on the Sherwood number, micro-organism Sherwood number, and velocity is elucidated in Figures 21–23. Upon elevating the Lewis number, both concentration and the micro-organism profile diminish, which is juxtaposed with an enhancement in fluid velocity. This phenomenon can be linked to the reduction in mass that followed diffusivity rate resulting from the heightened Lewis number. As the mass diffusivity decreases, it signifies that the transferred substance, whether it be a chemical species or micro-organisms, diffuses at a more gradual pace relative to the rate at which temperature propagates.

To ensure both numerical accuracy and result validation, our findings have been cross verified with the results reported by Lai et al. [35] and C.S.K et al. [31], as presented in Table 1.

Table 1. Comparison of the result for local Nusselt number and Sherwood number when $Nr = Nb = Nt = 0$.

Le	N	$\left(Nu(Nr)^{-0.5}\right)$ Lai et al. [35]	$\left(Sh(Nr)^{-0.5}\right)$ Lai et al. [35]	$\left(Nu(Nr)^{-0.5}\right)$ C.S.K et al. [31]	$\left(Sh(Nr)^{-0.5}\right)$ C.S.K et al. [31]	$\left(Nu(Nr)^{-0.5}\right)$ Present	$\left(Sh(Nr)^{-0.5}\right)$ Present
0.1	6	0.2868	0.0682	0.2896	0.0719	0.2867	0.0619
	4	0.2384	0.0594	0.2454	0.0599	0.2484	0.0580
	2	0.1824	0.0540	0.1862	0.0439	0.1826	0.0499
	0	0.1368	0.0168	0.0909	0.0156	0.0909	0.0155
1.0	6	0.2296	0.2296	0.2379	0.2381	0.2379	0.2396
	4	0.1976	0.1976	0.2014	0.2014	0.1914	0.2010
	2	0.1648	0.1648	0.1557	0.1567	0.1548	0.1597
	0	0.1368	0.1368	0.0909	0.0900	0.1368	0.0909

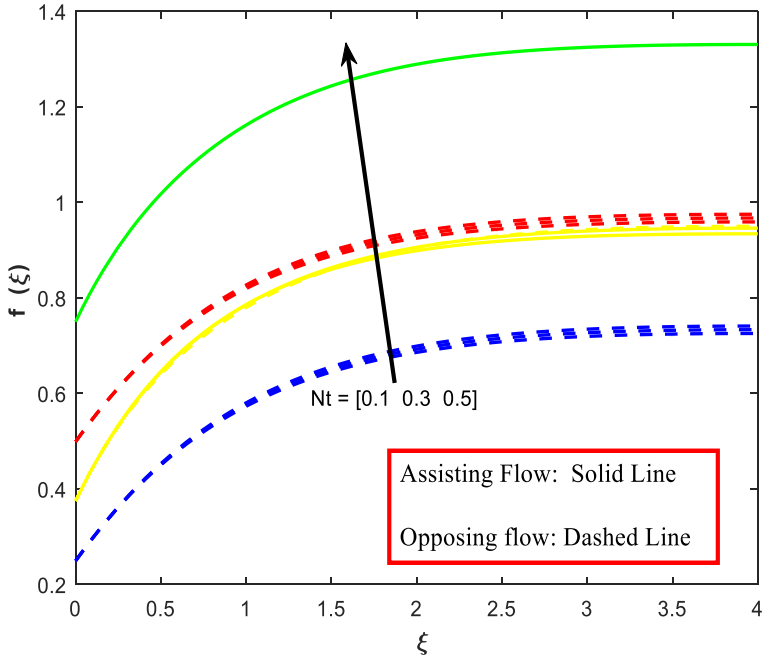

Figure 3. The impact of Nt on $f(\xi)$.

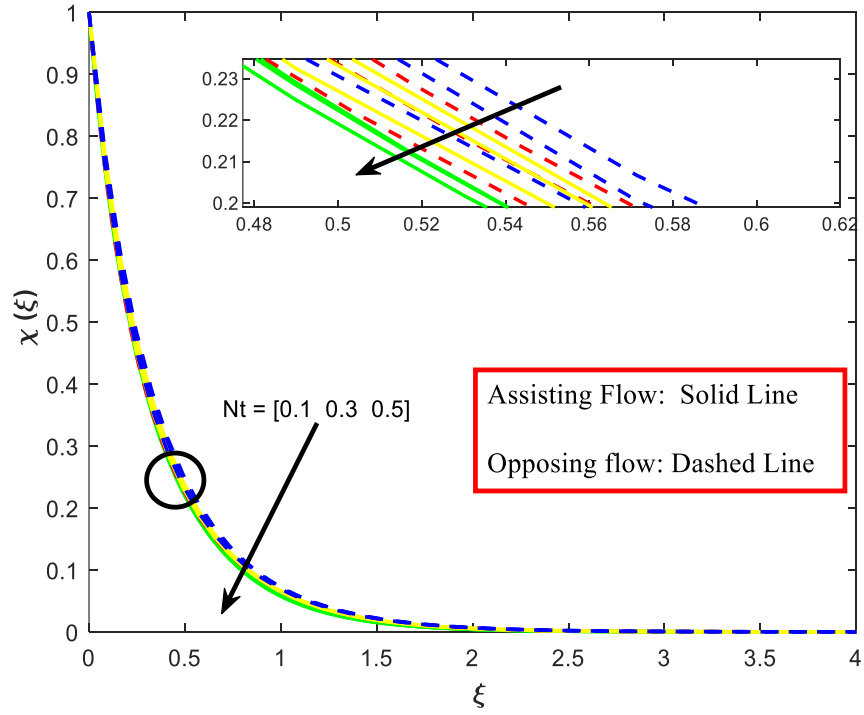

Figure 4. The influence of Nt on $\chi(\xi)$.

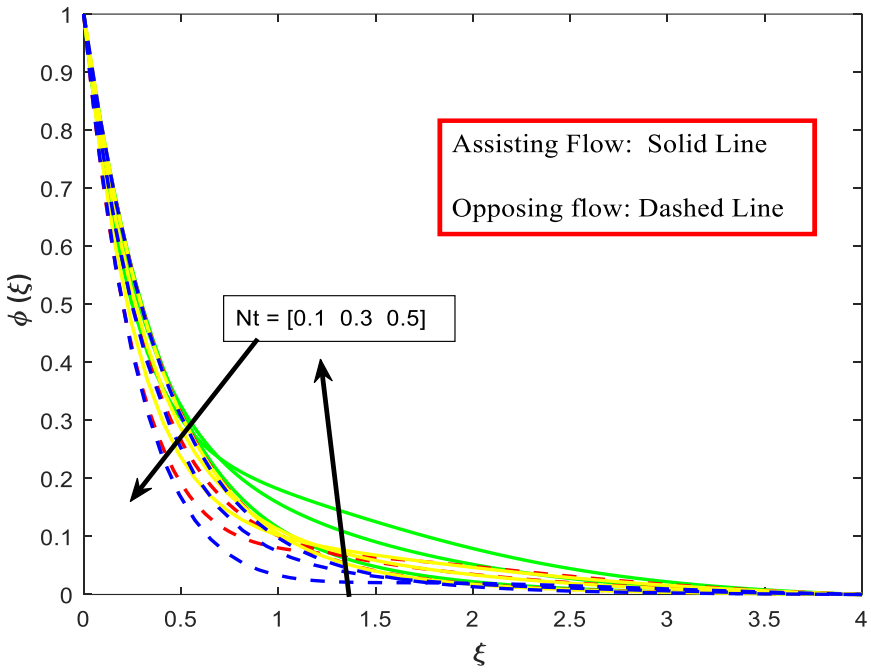

Figure 5. The influence of Nt on $\phi(\xi)$.

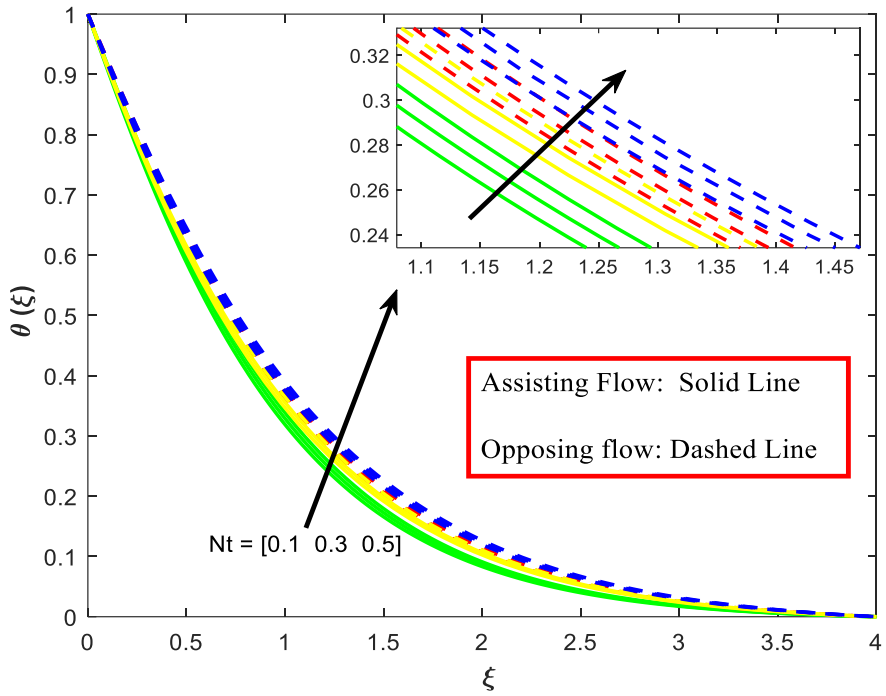

Figure 6. The influence of Nt on $\theta(\xi)$.

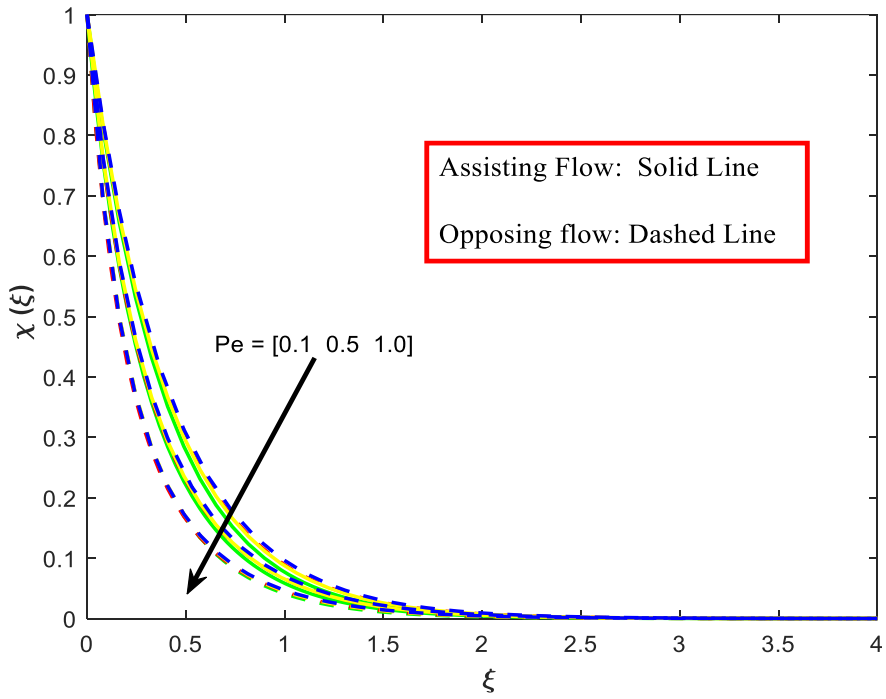

Figure 7. The influence of Pe on $\chi(\xi)$.

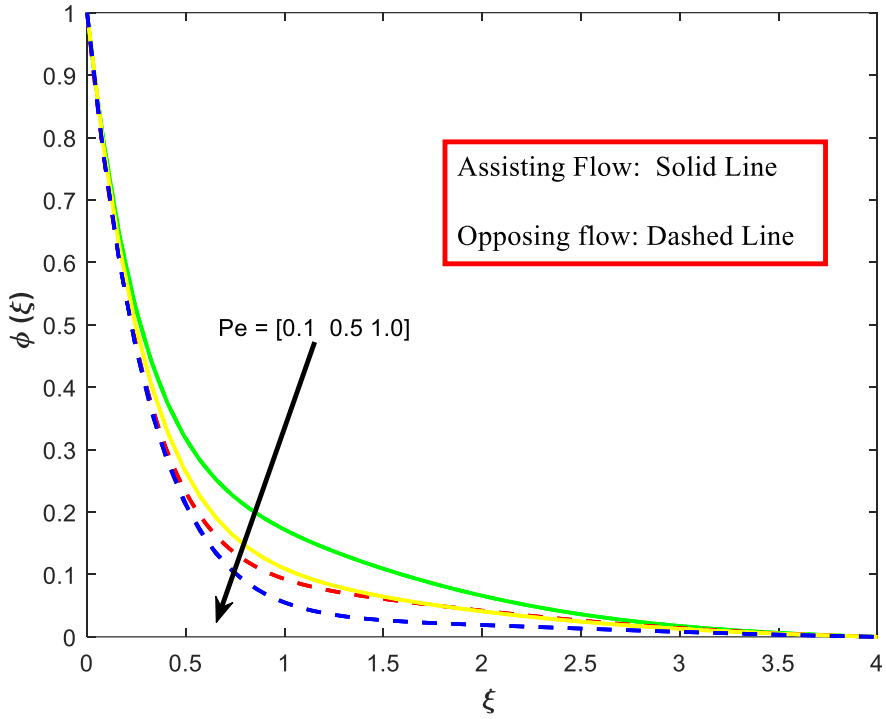

Figure 8. The influence of Pe on $\phi(\xi)$.

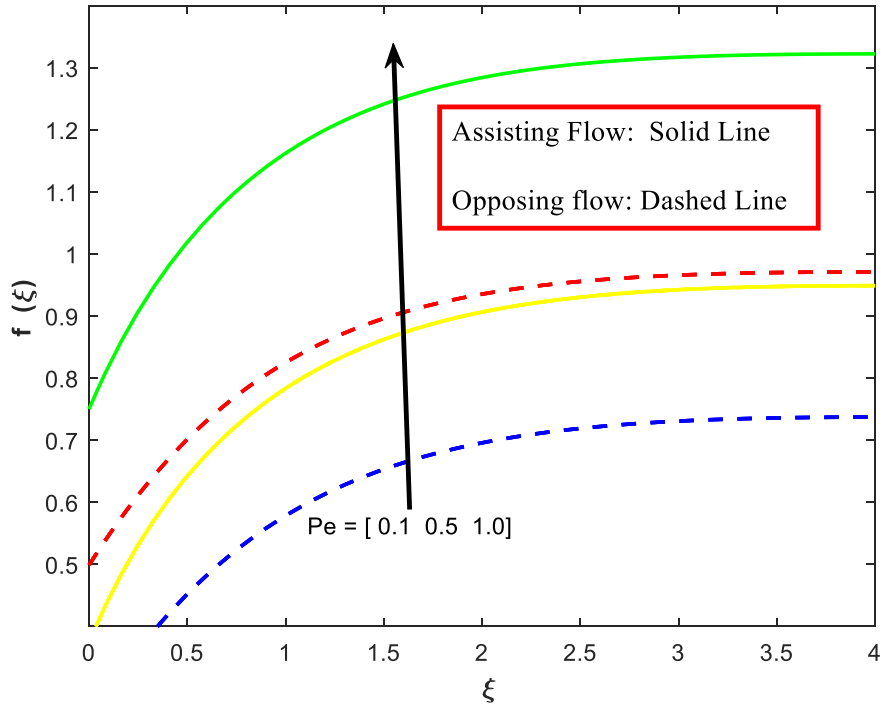

Figure 9. The effect of Pe on $f(\xi)$.

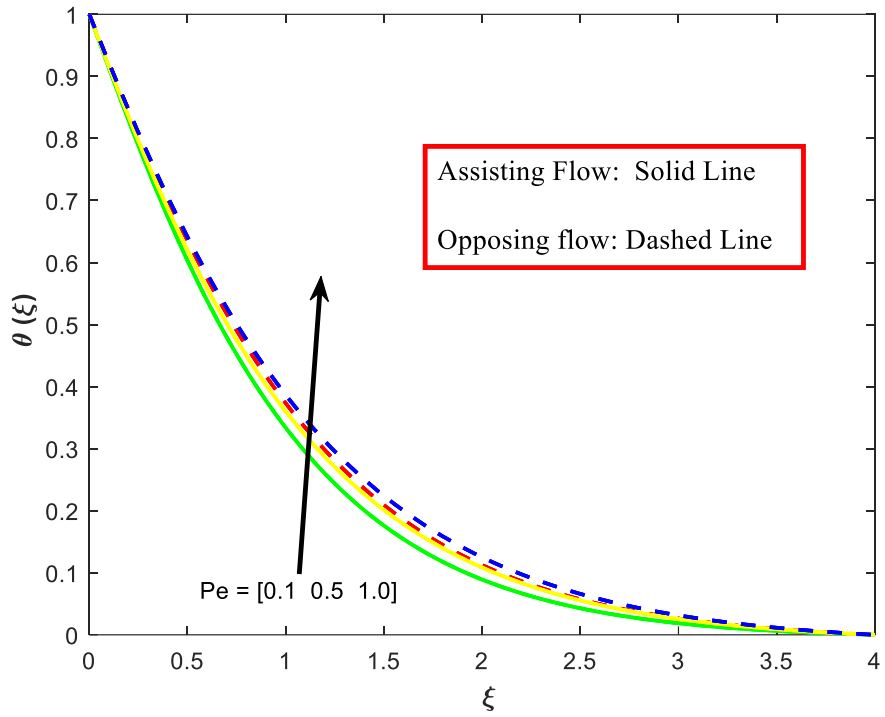

Figure 10. The influence of Pe on $\theta(\xi)$.

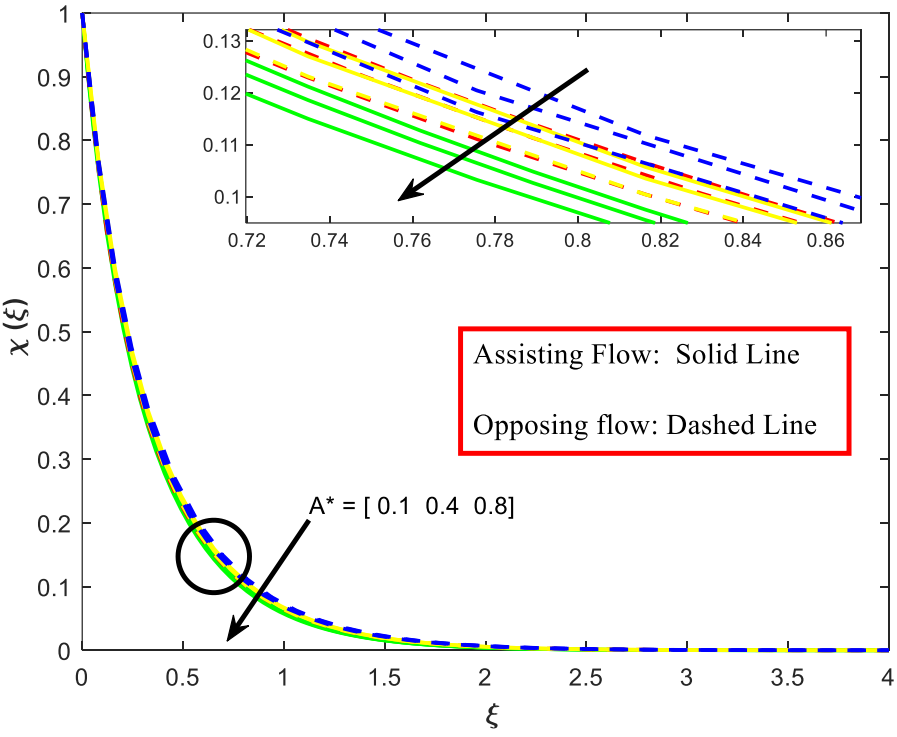

Figure 11. The impact of A^* on $\chi(\xi)$.

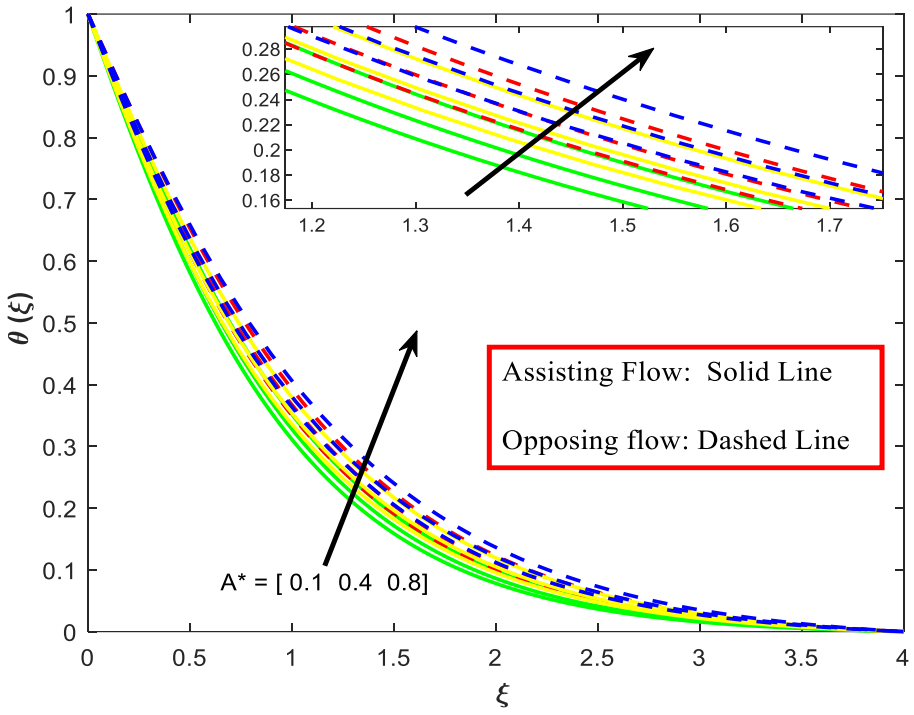

Figure 12. The influence of A^* on $\theta(\xi)$.

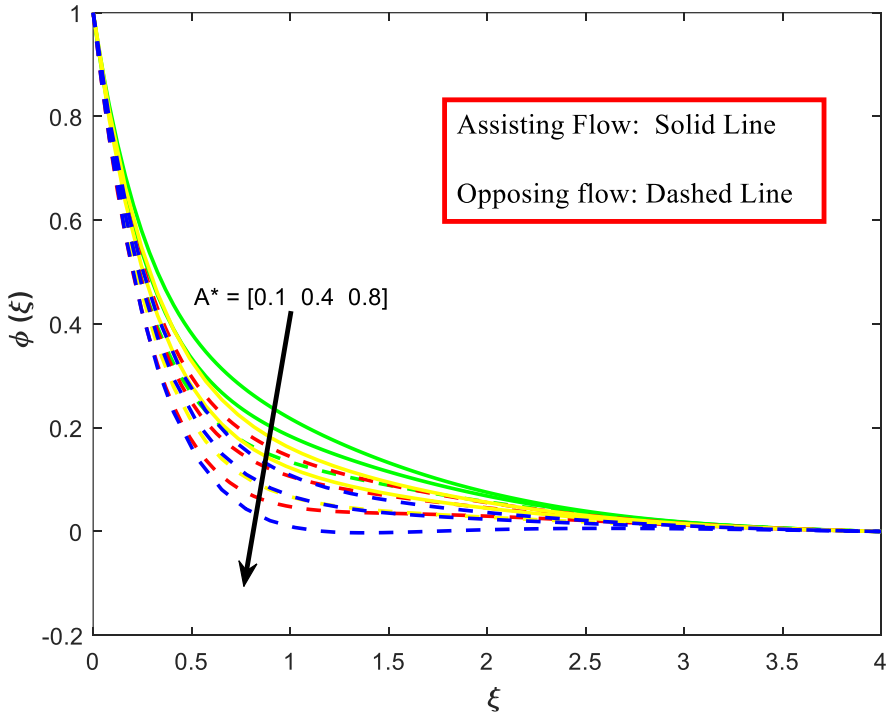

Figure 13. The influence of A^* on $\phi(\xi)$.

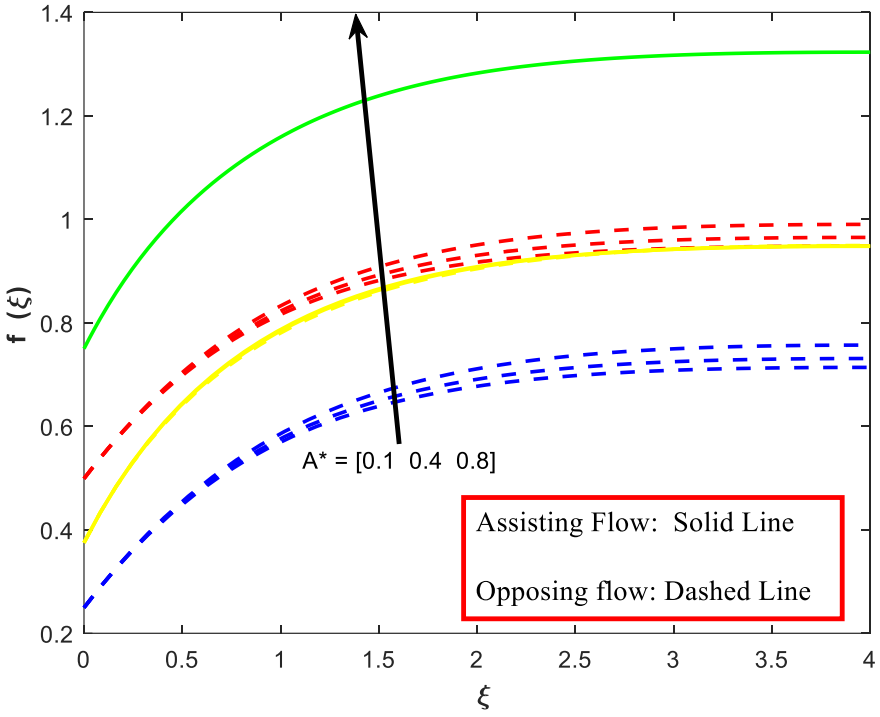

Figure 14. The influence of A^* on $f(\xi)$.

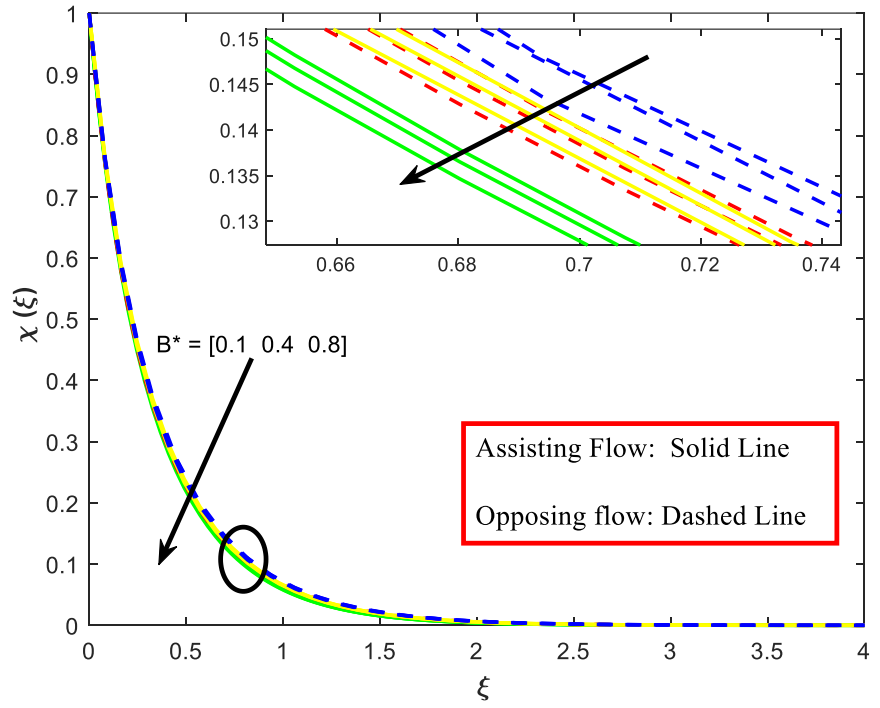

Figure 15. The effect of B^* on $\chi(\xi)$.

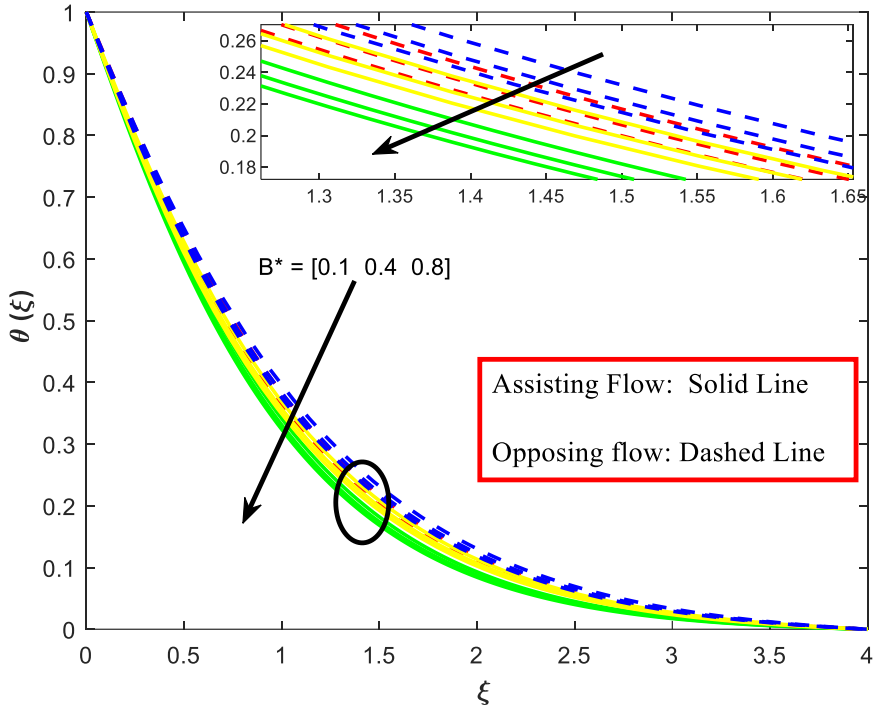

Figure 16. The impact of B^* on $\theta(\xi)$.

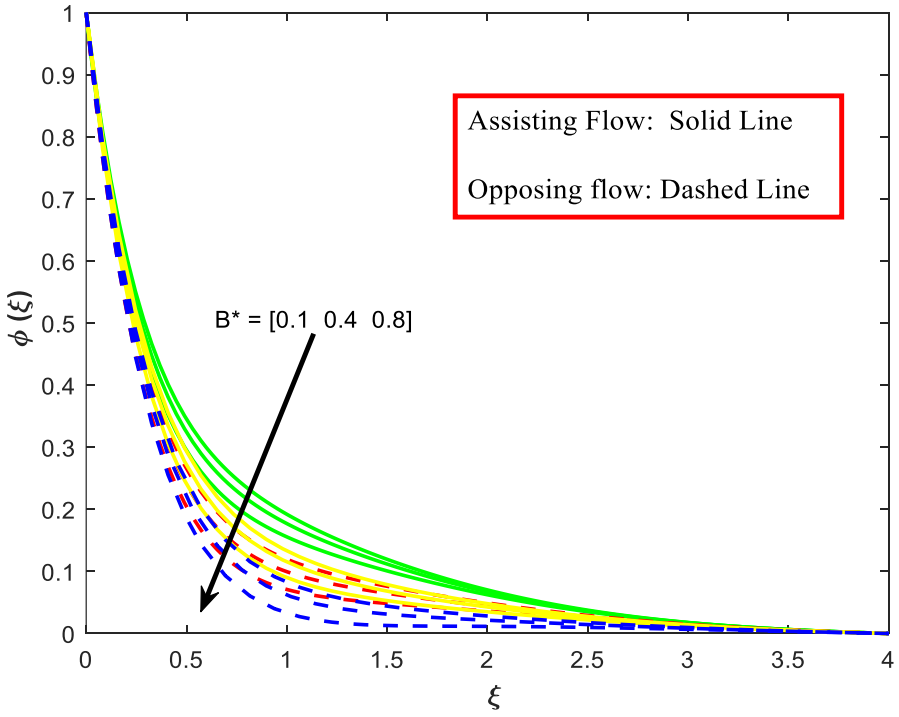

Figure 17. The influence of B^* on $\phi(\xi)$.

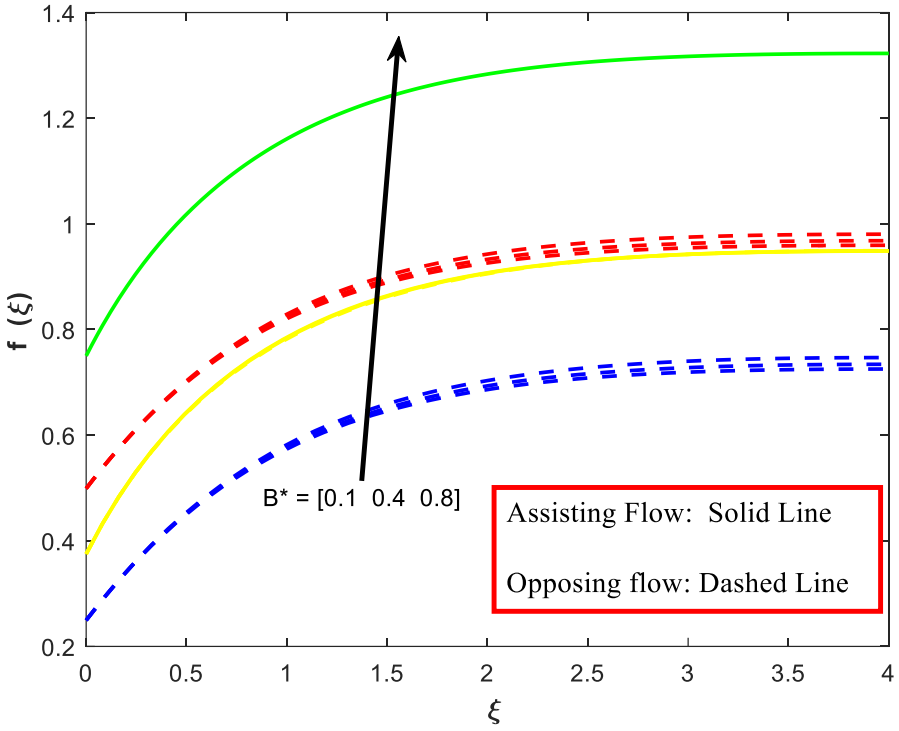

Figure 18. The effect of B^* on $f(\xi)$.

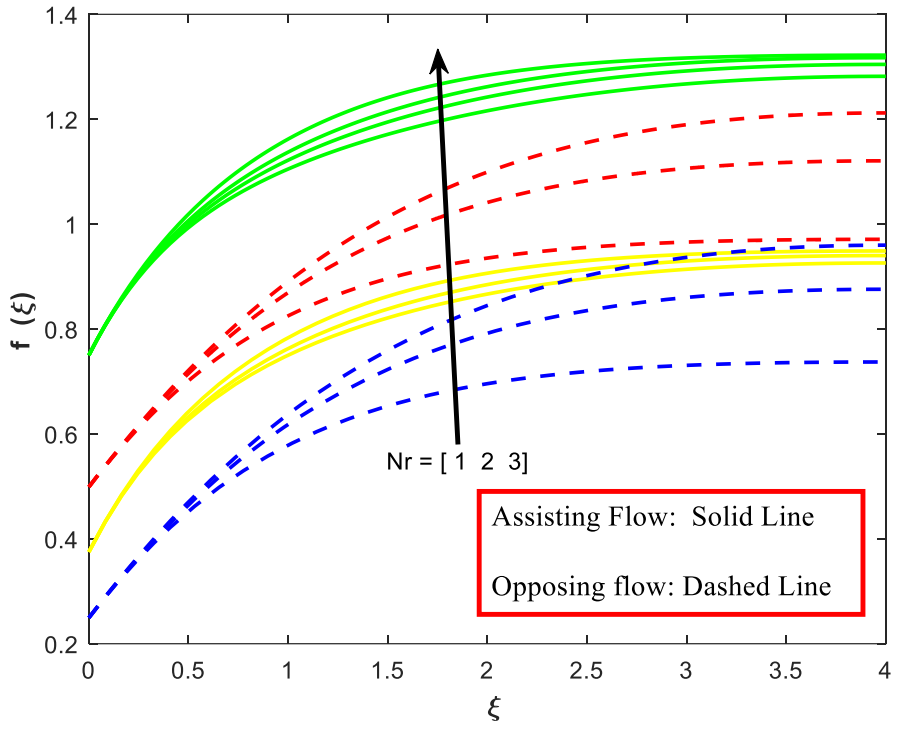

Figure 19. The influence of Nr on $f(\xi)$.

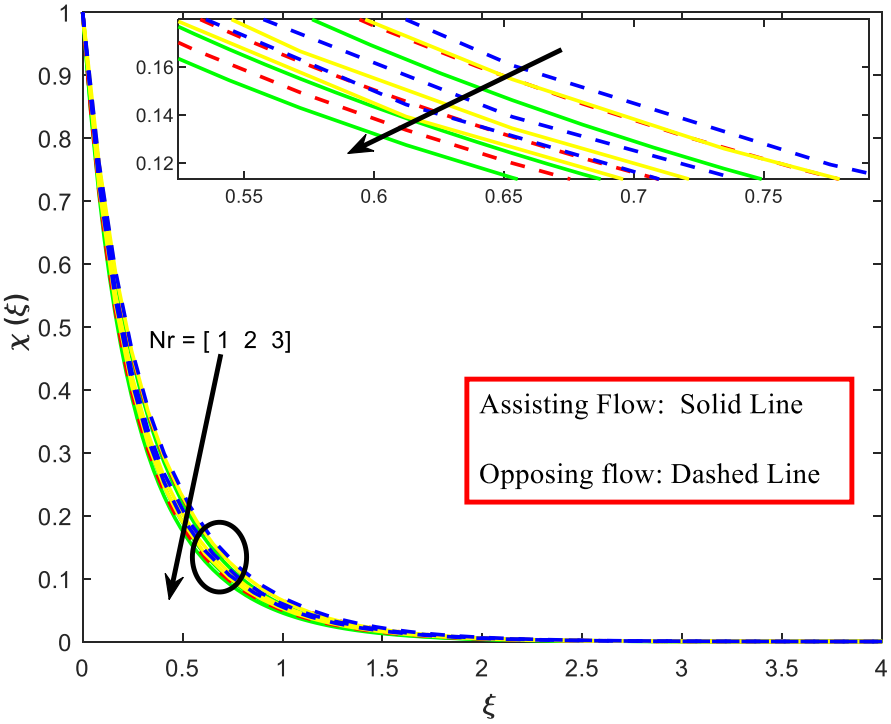

Figure 20. The impact of Nr on $\chi(\xi)$.

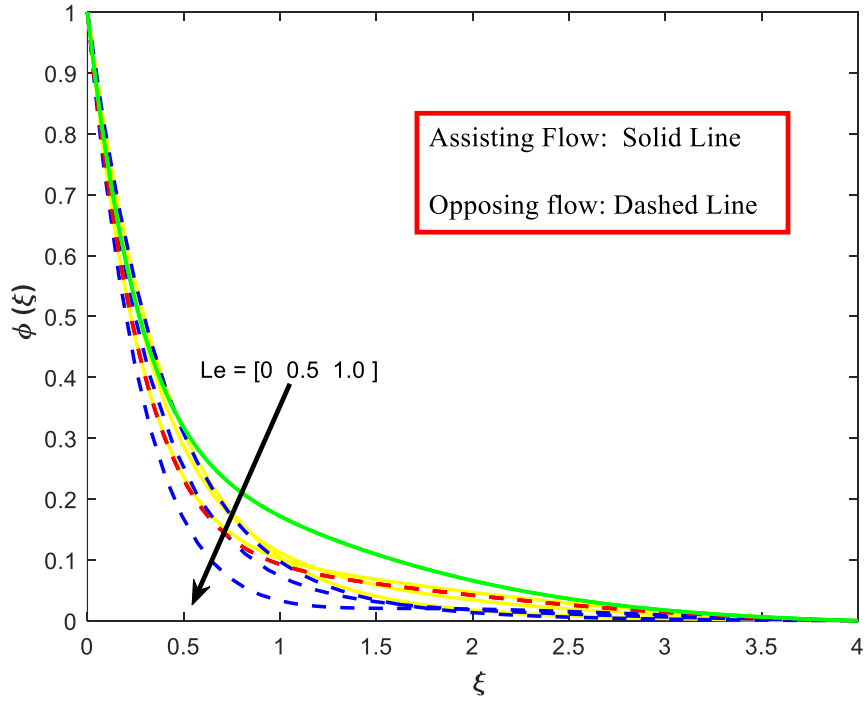

Figure 21. The effect of Le on $\phi(\xi)$.

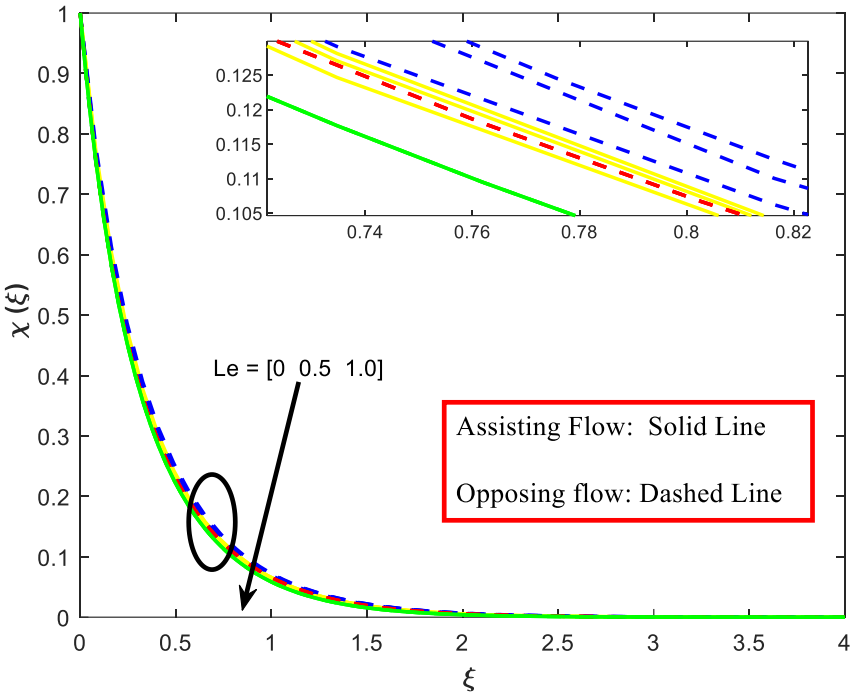

Figure 22. The influence of Le on $\chi(\xi)$.

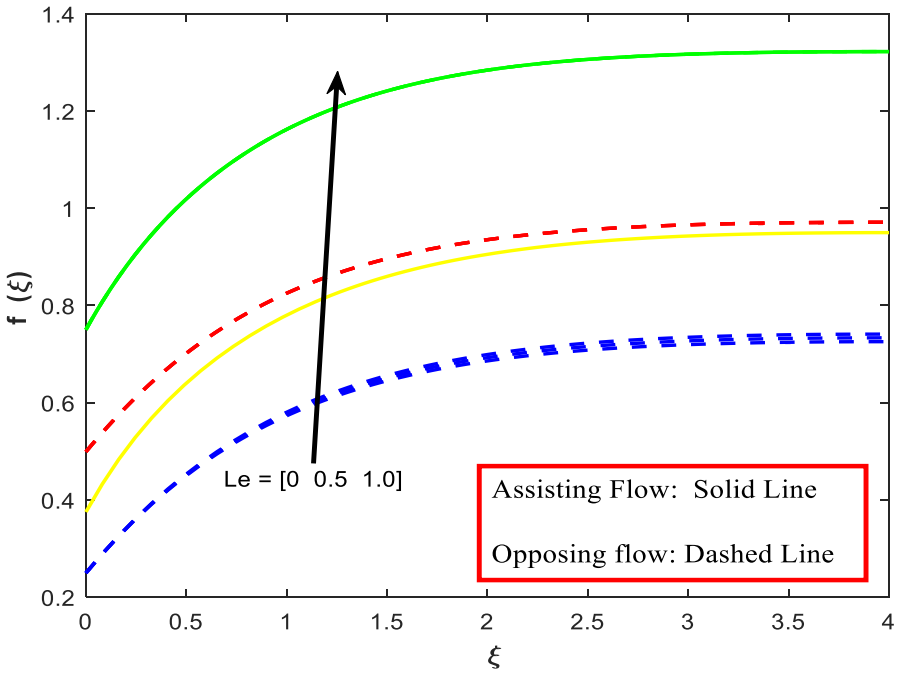

Figure 23. The impact of Le on $f(\xi)$.

Table 2. Multilinear regression data for Nusselt number for assisting and opposing flow for both cases.

Nr	Le	Pe	Nb	Nt	A^*	B^*	$Nus1$ cone $Nc = 0.5$	$Nus2$ cone $Nc = -0.0023$	$Nus3$ Cylinder $Nc = 0.5$	$Nus4$ Cylinder $Nc = -0.0023$
1	0	0.1	0.1	0.1	0.1	0.2	1.112398	1.01407	1.082325	1.009811
1.5	0.8	0.6	0.2	0.2	0.4	0.1	0.808605	0.719776	0.765431	0.733195
3	0.2	1	0.6	0.4	0.8	0.6	0.419557	0.353955	0.411827	0.391574
0.5	1	0.4	0.3	0.3	0.6	0.8	1.201475	67.59931	1.139925	11.51458
2	0.4	0.8	1	0.5	0.2	0.4	0.540037	0.490482	0.551049	0.520648

Table 3. Multilinear regression analysis result for Sherwood number for assisting and opposing flow for both cases.

Nr	Le	Pe	Nb	Nt	A^*	B^*	$Shr1$ cone $Nc = 0.5$	$Shr2$ cone $Nc = -0.0023$	$Shr3$ Cylinder $Nc = 0.5$	$Shr4$ Cylinder $Nc = -0.0023$
1	0	0.1	0.1	0.1	0.1	0.2	2.161306	2.268339	2.29304	2.333816
1.5	0.8	0.6	0.2	0.2	0.4	0.1	6.291796	8.129897	7.230078	7.8499
3	0.2	1	0.6	0.4	0.8	0.6	6.371352	6.862992	6.366014	6.421437
0.5	1	0.4	0.3	0.3	0.6	0.8	2.130939	-202.274	2.321761	-37.8
2	0.4	0.8	1	0.5	0.2	0.4	3.476704	3.53531	3.406319	3.421397

Table 4. Multilinear regression data for micro-organism Sherwood for assisting and opposing flow for both cases.

Nr	Le	Pe	Nb	Nt	A^*	B^*	$NShr1$ cone $Nc = 0.5$	$NShr2$ cone $Nc = -0.0023$	$NShr3$ Cylinder $Nc = 0.5$	$NShr4$ Cylinder $Nc = -0.0023$
1	0	0.1	0.1	0.1	0.1	0.2	2.774389	2.580463	2.632089	2.498268
1.5	0.8	0.6	0.2	0.2	0.4	0.1	5.443797	6.422092	5.89567	6.228125
3	0.2	1	0.6	0.4	0.8	0.6	2.679446	2.666468	7.776058	7.797635
0.5	1	0.4	0.3	0.3	0.6	0.8	3.456229	-85.5357	3.306591	-6.36953
2	0.4	0.8	1	0.5	0.2	0.4	4.684654	4.612654	4.530898	4.47172

The use of a color-coding system, Green, Blue, Red, and Cyan, distinguishes two types of flows, assisting and opposing, in slender structures like cones and cylinders. Specifically, in the case of a cone, green represents assisting flow, while red signifies opposing flow. Similarly, in the context of a cylinder, blue denotes assisting flow, and cyan indicates opposing flow. Tables 2, 3, and 4 were utilized to develop 3D graphs showing fluid flow conditions for Nu, Shr and $NShr$.

Figures 24–26 illustrate the change in the Nusselt number (Nu), which signifies the surface heat transfer rate. As shown in Figure 24, increasing the thermophoresis parameter (Nt) leads to a decrease in Nu, particularly in cone geometries, due to enhanced nanoparticle migration away from the heated

surface, which weakens the thermal gradient. Brownian motion (Nb) shows a relatively minor effect. Figure 25 highlights that increasing the radiation parameter (Nr) reduces Nu by diverting more energy into radiation rather than conduction. In contrast, the Lewis number (Le) slightly improves Nu by maintaining stronger temperature gradients. Figure 26 demonstrates that higher values of the non-uniform heat source (A) and sink (B) parameters cause a decline in Nu, as internal energy disturbances weaken the surface temperature gradient, reducing conductive heat transfer.

Figures 27–29 focus on the Sherwood number (Sh), a measure of mass transfer. Figure 27 shows that both Peclet number (Pe) and Lewis number (Le) significantly enhance Sh. Higher Pe intensifies advective transport, while increased Le suppresses diffusion, thus sharpening concentration gradients near the surface. Figure 28 shows that thermophoresis (Nt) strongly enhances Sh by directing nanoparticles along thermal gradients, while Nb has a varied or less predictable impact. Figure 29 reveals that the inclusion of internal heating (A) and absorption (B) generally enhances mass transfer (Sh), especially for the cylinder in opposing flow, due to the modification of thermal fields which influence species diffusion.

Figures 30–32 depict the microorganism Sherwood number $(NShr)$, reflecting the rate of bioconvective mass transport. Figure 30 shows that higher Pe and Le lead to a strong increase in $NShr$ by enhancing advection and reducing microbial dispersion. Figure 31 confirms that the non-uniform heat source/sink parameters (A) and (B) stimulate microorganism activity and thus increase $NShr$, particularly in opposing flow scenarios. Finally, Figure 32 indicates that thermophoresis (Nt) boosts $NShr$ by encouraging microorganism movement along temperature gradients, while Brownian motion (Nb) introduces irregularity and has a smaller influence.

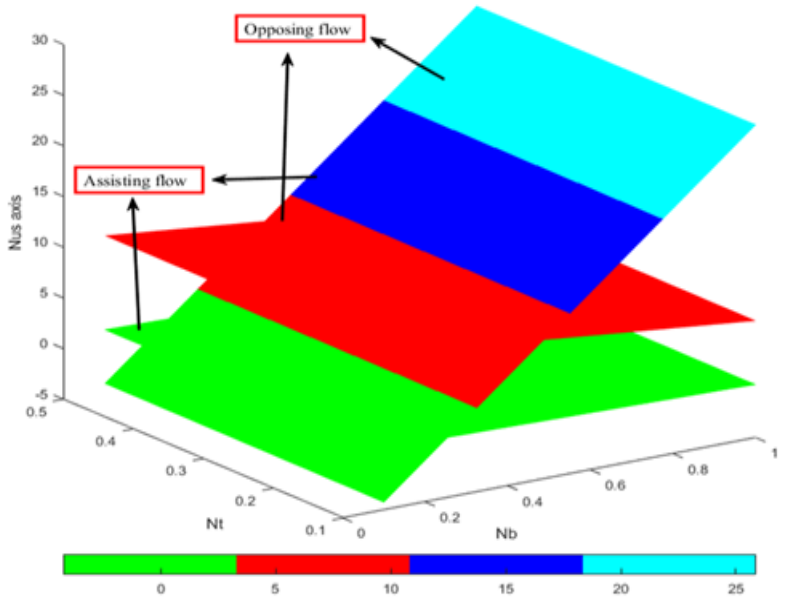

Figure 24. The influence of Nb and Nt on Nus.

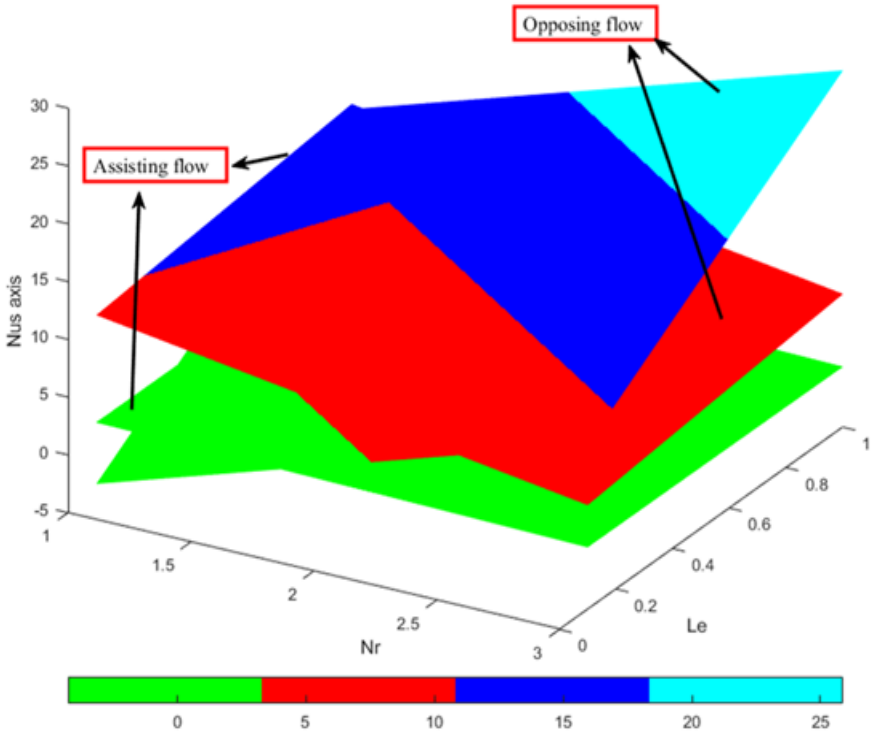

Figure 25. The impact of Nr and Le on Nus.

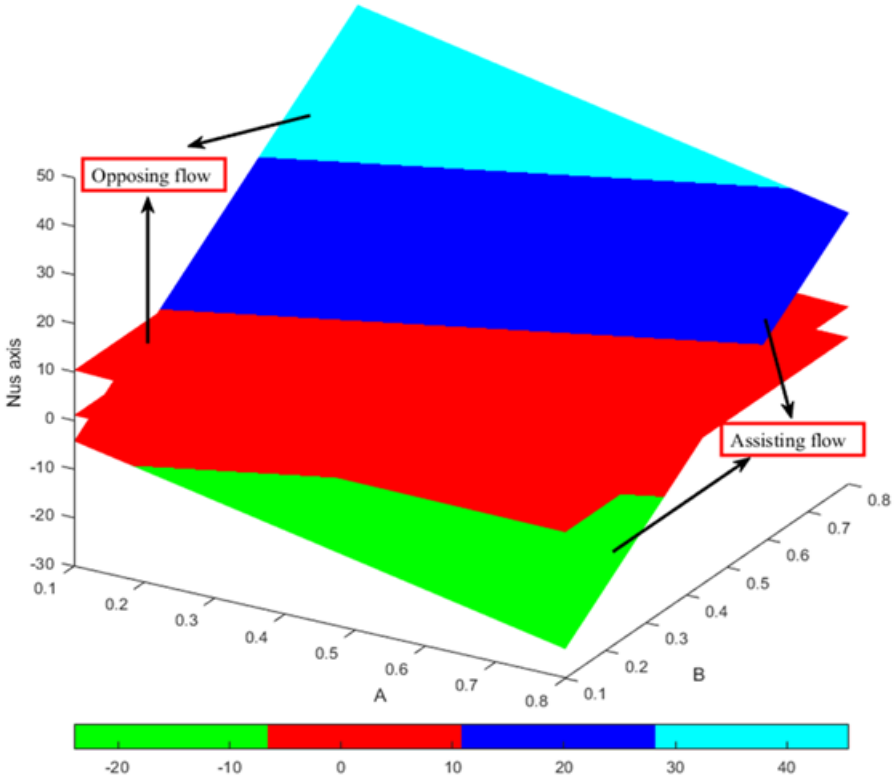

Figure 26. The impact of A and B on Nus.

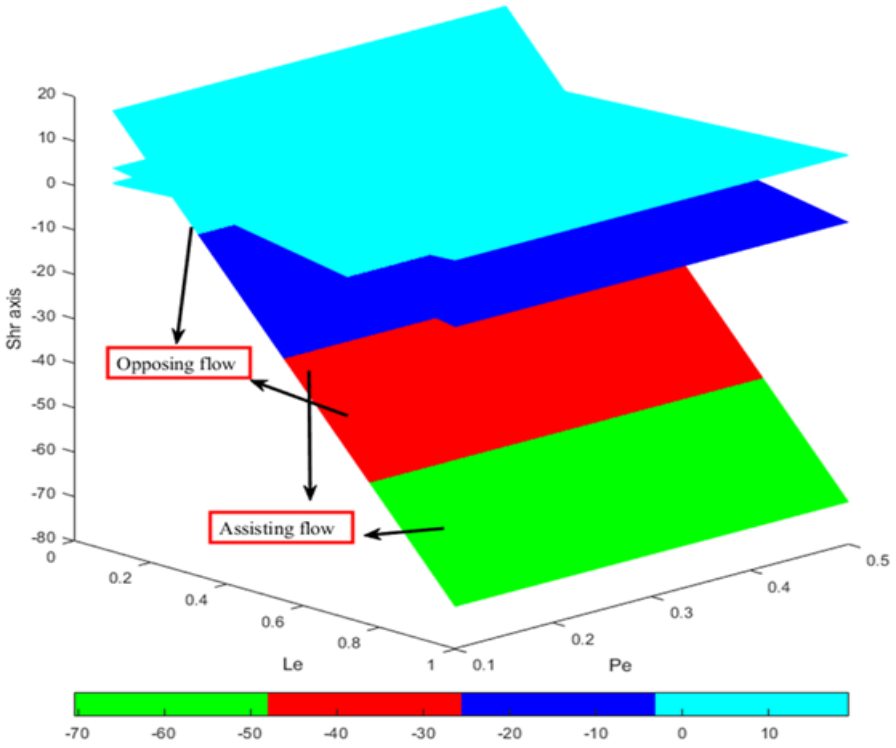

Figure 27. The effect of Le and Pe on Shr.

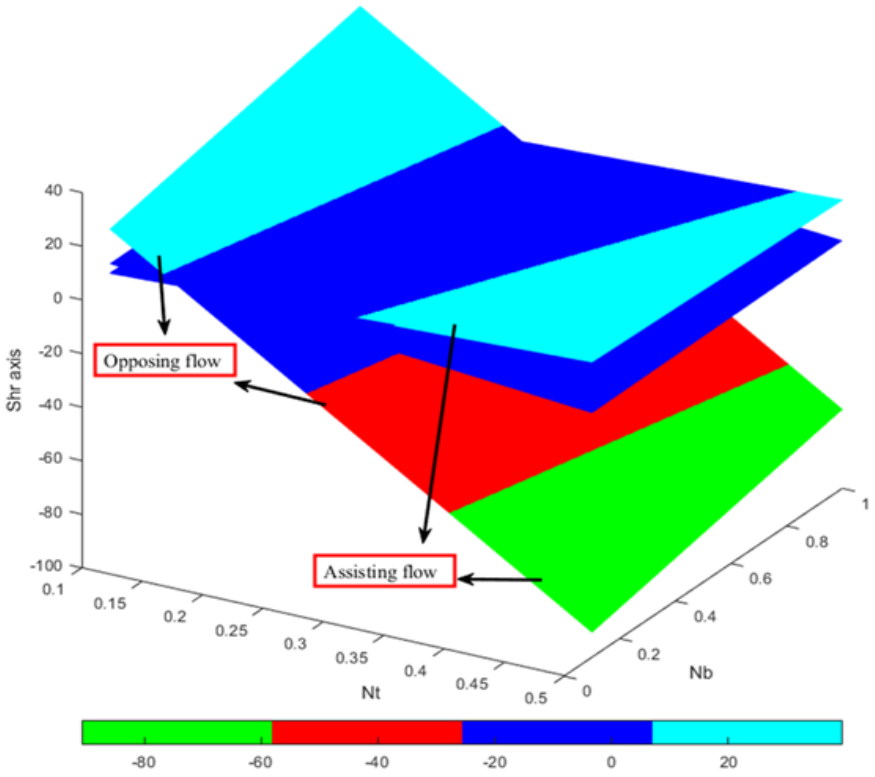

Figure 28. The impact of Nt and Nb on Shr.

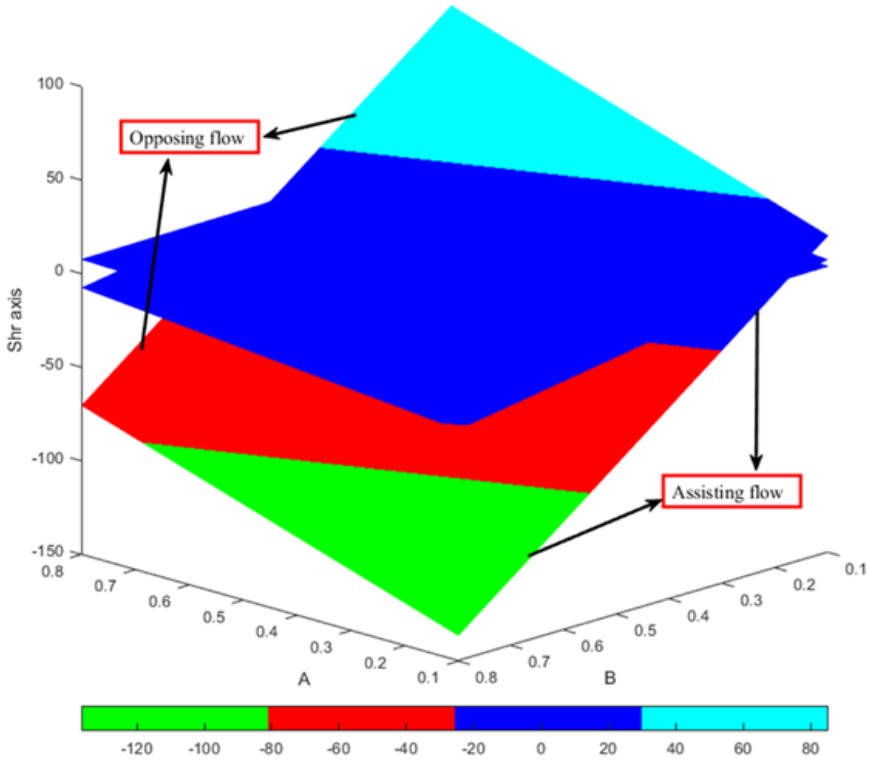

Figure 29. The influence of A and B on Shr.

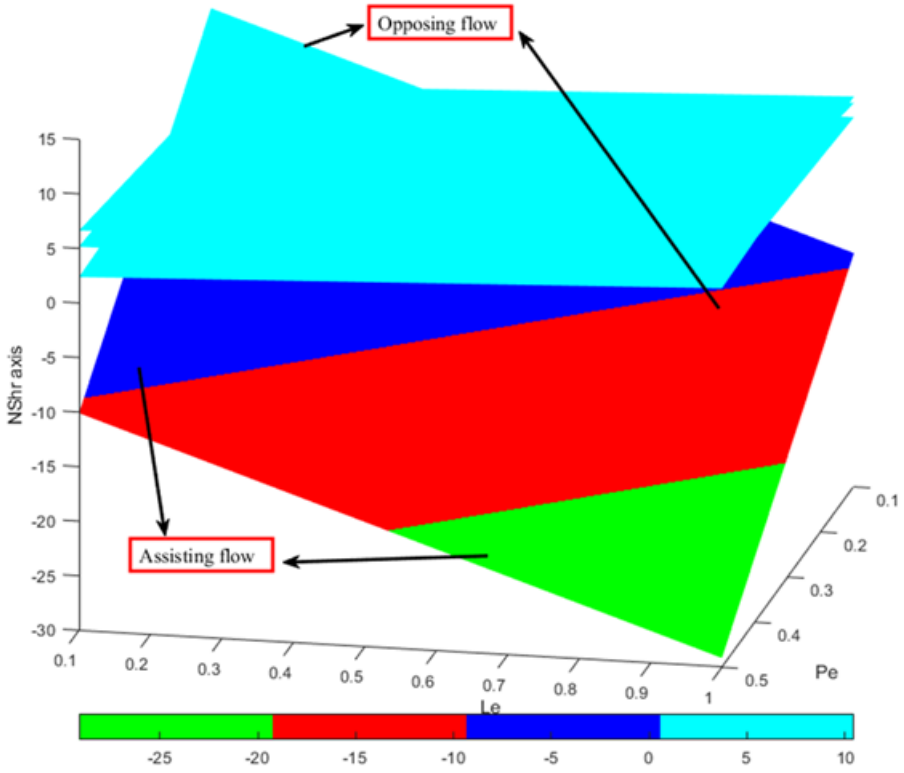

Figure 30. The effect of Le and Pe on NShr.

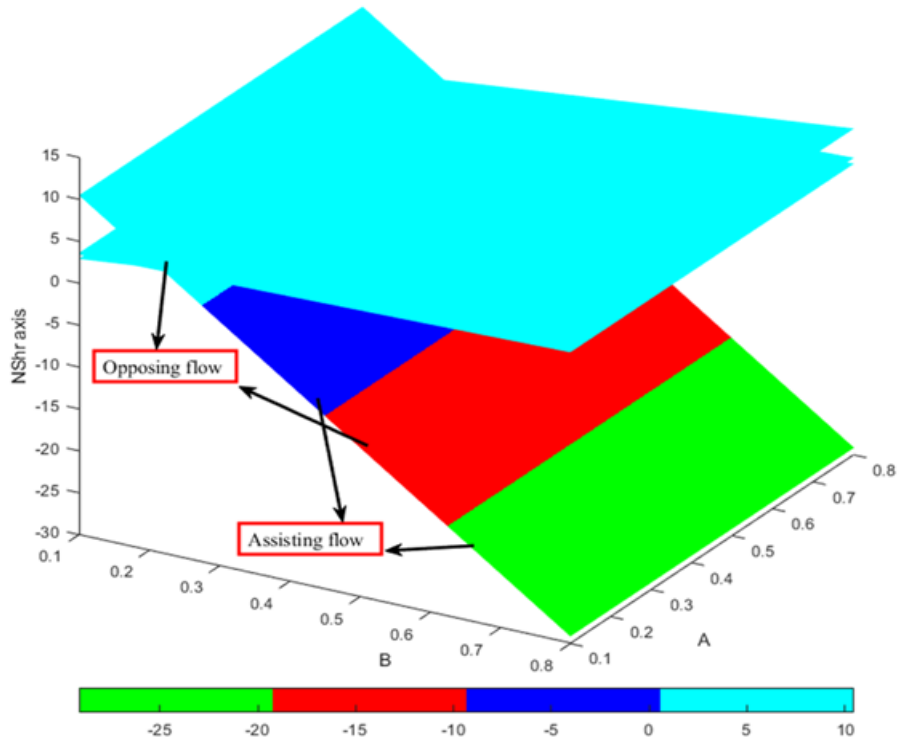

Figure 31. The influence of A and B on NShr.

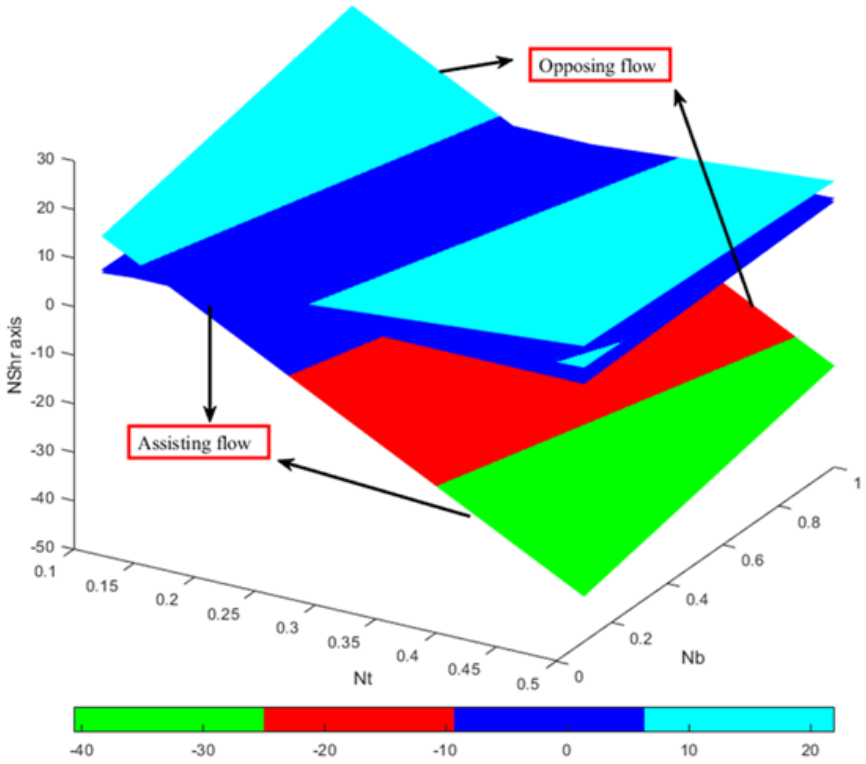

Figure 32. The impact of Nt and Nb on NShr.

Table 5. Governing physical quantities for various values of $Nt = 0.4, Nb = 0.4, B^* = 0.5, A^* = 0.5, Nr = 01, Le = 0.5, Pe = 0.5, n = 0.5$ in assisting the flow.

Nt	Le	Pe	A^*	B^*	Nr	Nu		Sh		NSh	
						Cone	Cylinder	Cone	Cylinder	Cone	Cylinder
0.1						0.936610	0.914634	2.346142	2.388930	3.334658	3.248478
0.3						0.893111	0.873751	2.621408	2.709172	3.472373	3.400226
0.5						0.850353	0.832322	3.074504	3.192849	3.690678	3.625529
	0.0					0.871621	0.914634	2.826054	2.388930	3.571269	3.248478
	0.5					0.871621	0.873751	2.826054	2.709172	3.571269	3.400226
	1.0					0.871621	0.832322	2.826054	3.192849	3.571269	3.625529
		0.0				0.871622	0.853089	2.826053	2.930404	2.609680	2.525751
		0.5				0.871621	0.853089	2.826054	2.930404	3.571269	3.503556
		1.0				0.871622	0.853089	2.826053	2.930404	4.817911	4.779568
			0.1			0.952049	0.931540	2.485225	2.620443	3.417831	3.367162
			0.4			0.891974	0.872951	2.739694	2.851869	3.532393	3.469005
			0.8			0.809514	0.792436	3.090078	3.170486	3.690102	3.609154
				0.1		0.906188	0.887856	2.679465	2.793007	3.505286	3.443246
				0.4		0.880386	0.861914	2.788860	2.895514	3.554504	3.488247
				0.8		0.844808	0.826045	2.939957	3.037376	3.622481	3.550469
					1	0.871621	0.853089	2.826054	2.930404	3.571269	3.503556
					2	0.593760	0.596951	4.092433	3.981448	4.122382	3.948139
					3	0.478809	0.487323	4.667860	4.462841	4.370596	4.149650

Table 6. Governing physical quantities for various values of $Nt = 0.4, Nb = 0.4, B^* = 0.5, A^* = 0.5, Nr = 01, Le = 0.5, Pe = 0.5, n = 0.5$ for opposing the flow.

Nt	Le	Pe	A^*	B^*	Nr	Nu		Sh		NSh	
						Cone	Cylinder	Cone	Cylinder	Cone	Cylinder
0.1						0.847603	0.852555	2.339997	2.365953	3.198662	3.149074
0.3						0.805256	0.812232	2.807329	2.811394	3.419209	3.355536
0.5						0.763335	0.772315	3.447896	3.414237	3.719812	3.634299
	0.0					0.784224	0.852555	3.106202	2.365953	3.559569	3.149074
	0.5					0.784224	0.812232	3.106202	2.811394	3.559569	3.355536
	1.0					0.784224	0.772315	3.106202	3.414237	3.559569	3.634299
		0.0				0.784224	0.792208	3.106202	3.093352	2.505707	2.454196
		0.5				0.784224	0.792208	3.106202	3.093352	3.559569	3.485939
		1.0				0.784224	0.792208	3.106202	3.093352	4.932279	4.836608
			0.1			0.858884	0.862499	2.791520	2.811891	3.418956	3.360877
			0.4			0.803485	0.810295	3.024820	3.020961	3.523226	3.453791
			0.8			0.723748	0.735652	3.362682	3.319544	3.674048	3.586285
				0.1		0.822357	0.828046	2.945218	2.949890	3.487670	3.422220
				0.4		0.793910	0.801301	3.065255	3.056963	3.541288	3.469780
				0.8		0.754499	0.764367	3.232081	3.204734	3.615764	3.535353
					1	0.784224	0.792208	3.106202	3.093352	3.559569	3.485939
					2	0.533314	0.565406	4.269544	4.027273	4.061488	3.886222
					3	0.431804	0.468091	4.811542	4.440980	4.293866	4.061622

Tables 5 and 6 present the variations in the Nusselt number (Nu), Sherwood number (Sh), and micro-organisms Sherwood number $(NShr)$. I have fixed the values of $Nc = 0.5$ for assisting flow and $Nc = -0.0023$ for opposing flow and $Nt = 0.4, Nb = 0.4, B^* = 0.5, A^* = 0.5, Nr = 01, Le = 0.5, Pe = 0.5, n = 0.5$ in both the assisting and opposing flow cases. Elevating the Thermophoresis parameter (Nt) and radiation parameters (Nr) results in an increase in the Sherwood number and micro-organisms Sherwood number for both assisting and opposing flows, followed by a decline in the Nusselt number in both cases. As anticipated, an increase in thermal radiation enhances heat molecules in the flow, resulting in a significant improvement in mass transfer rate was identified.

Regarding the Peclet number (Pe) and Lewis number (Le), the rates of heat and mass transfer remain constant. However, an enhancement in (Pe) and (Le) values exhibit an enhancing effect on the diffusivity of micro-organisms in both cases. Furthermore, escalating the values of non-uniform heat generation and absorption parameters (A^* and B^*) promote a growth in the Sherwood number

and micro-organisms Sherwood number, while causing a decrease in heat transfer values for both assisting and opposing flows.

4. Conclusions

The field of bio-convection, which is highly captivating, has attracted considerable interest due to its numerous applications in areas such as medicine, cancer treatment, water distillation, advanced aircraft manufacturing, modern defense equipment, enhanced electronic instruments, efficient batteries, and cosmetics production. Recognizing the extensive relevance of this field, a numerical study was conducted to investigate buoyancy-driven flow incorporating thermal and diffusion processes in a saturated Darcy medium. Different factors, including Brownian motion, thermal radiation, thermophoresis, and gyrotactic organisms, were meticulously examined to understand their impacts under two specific scenarios: Flow around a cylinder and a cone with both assisting and opposing flow. The physical model was initially represented by a set of complex and nonlinear partial differential equations, which were subsequently reduced to a more tractable system of ordinary differential equations using suitable similarity transformations. These equations were solved systematically using the Runge-Kutta approach to solve the transformed equations numerically. The flow variables were modeled using the multilinear regression method to obtain solutions. The study culminated in visually striking graphical representations detailing the complexities of two geometries: Cone and cylinder (assisting and opposing flow). These stream function and temperature plots and numerical findings for important flow and heat transfer parameters in tabular form for the flow dynamics reveal key physical properties of the system, particularly diffusion and thermal distributions, as well as rates of heat and mass transfer. An important outcome of the study indicated that microorganisms play a crucial role in enhancing mass transfer, with rates markedly higher than in their absence. Practical applications of our study are microbial bioreactors and biosensors, where gyrotactic microorganisms enhance mass transport. Cooling of electronic components in porous enclosures, where thermal radiation and convective flows are critical and biomedical fluid transport systems shows that, in drug delivery through porous tissues, the non-uniform heat sources/sinks and suspended microbes influence thermal gradients. A summary of the primary findings from this investigation is provided here.

I. The rate of heat transfer experiences a downturn with Nt, Le, Nr, A^* and B^* for both the scenario assisting flow and opposing flow in both the cone and the cylinder cases.

II. Within the context of the cylinder scenario, it can be observed that the Sherwood number exhibits a decrease in value in comparison to situations where micro-organisms are present, particularly with the escalation of the heat radiation parameter levels.

III. An increment in the radiation parameter (Nr) leads to enhanced fluid velocity and a reduction in microorganism concentration profiles for both assisting and opposing flow scenarios.

IV. The influence of the Peclet number on heat transfer is a consistent factor to consider. Nevertheless, noteworthy alterations in the Sherwood number relating to mass transfer are solely noticeable in cases involving micro-organisms, leading to a considerable rise in their numerical values.

The presence of micro-organisms significantly enhances the mass transfer rate in both assisting and opposing flow conditions for both cone and cylinder configurations. This highlights their vital

contribution to improving mass transfer efficiency within the studied flow systems.

Limitations and future directions:

While this study offers valuable insights, it has certain limitations, and future research can address these to enhance model accuracy and applicability.

- **Lack of experimental validation:**

Performing laboratory experiments or comparing results with existing experimental datasets to validate the model's predictive capabilities.

- **Simplified geometry:**

Only slender geometries (cone and cylinder) were considered, limiting generalizability to more complex or irregular shapes encountered in real systems.

- **Numerical validation:**

While a 4th-order Runge-Kutta method was used, no formal convergence, step-size sensitivity, or mesh independence study was performed. The accuracy of the results was inferred through consistency checks only.

- **Sensitivity analysis** to evaluate the influence of key physical parameters.
- **Simplified biological modeling**:

The gyrotactic microorganisms were modeled without accounting for species variation, size differences, reproduction, or time-dependent biological responses.

- **No statistical or error analysis in MLR:**

The multilinear regression (MLR) approach did not include statistical validation metrics (e.g., R^2, p-values, and confidence intervals) or uncertainty quantification.

- **Transient and turbulence effect:**

Investigating unsteady bio-convective flows, possibly with turbulence models or time-dependent biothermal simulations.

- **Complex geometry:**

Extending the framework to handle non-slender, irregular, or bio-inspired geometries using computational tools like finite element (FEM) or finite volume (FVM) methods.

Advanced regression models

- **Transient and turbulent effects:**

Investigating unsteady bio-convective flows, possibly with turbulence models or time-dependent biothermal simulations.

- **Sensitivity and uncertainty analysis.**

Performing formal sensitivity analysis and error quantification for a robust evaluation of how individual parameters influence the system behavior.

Use of Generative-AI tools declaration

The author(s) declare(s) they have not used Artificial Intelligence (AI) tools in the creation of this article.

Acknowledgements

This work was supported and funded by the Deanship of Scientific Research at Imam Mohammad Ibn Saud Islamic University (IMSIU) (grant number IMSIU-DDRSP2503).

Conflict of interest

The author declared no conflict of interest.

References

1. A. V. Kuznetsov, A. A. Avramenko, Effect of Small Particles on the Stability of Bioconvection in a Suspension of Gyrotactic Microorganisms in a Layer of Finite Depth, *Int. Commun. Heat Mass*, **31** (2004), 1–10. https://doi.org/10.1016/S0735-1933(03)00196-9
2. P. Geng, A. V. Kuznetsov, Effect of Small Solid Particles on the Development of Bioconvection Plumes, *Int. Commun. Heat Mass*, **31** (2004), 629–638. https://doi.org/10.1016/S0735-1933(04)00050-8
3. P. Geng, A. V. Kuznetsov, Settling of Bidispersed Small Solid Particles in a Dilute Suspension Containing Gyrotactic Micro-Organisms, *Int. J. Eng. Sci.*, **43** (2005), 992–1010. https://doi.org/10.1016/j.ijengsci.2005.03.002
4. P. Geng, A. V. Kuznetsov, Introducing the Concept of Effective Diffusivity to Evaluate the Effect of Bioconvection on Small Solid Particles, *Int. J. Transp. Phenom.*, **7** (2005)**,** 321–338.
5. A. V. Kuznetsov, The Onset of Bioconvection in a Suspension of Gyrotactic Microorganisms in a Fluid Layer of Finite Depth Heated from Below, *Int. Commun. Heat Mass*, **32** (2005), 574–582. https://doi.org/10.1016/j.icheatmasstransfer.2004.10.021
6. M. V. S. Rao, K. Gangadhar, A. J. Chamkha, et al., Bioconvection in a Convectional Nanofluid Flow Containing Gyrotactic Microorganisms over an Isothermal Vertical Cone Embedded in a Porous Surface with Chemical Reactive Species, *Arab. J. Sci. Eng.*, **46** (2021), 2493–2503. https://doi.org/10.1007/s13369-020-05132-y
7. A. V. Kuznetsov, Thermo-Bioconvection in a Suspension of Oxytactic Bacteria, *Int. Commun. Heat Mass*, **32** (2005), 991–999. https://doi.org/10.1016/j.icheatmasstransfer.2004.11.005
8. A. V. Kuznetsov, Investigation of the Onset of Thermo-Bioconvection in a Suspension of Oxytactic Microorganisms in a Shallow Fluid Layer Heated from Below, *Theor. Comput. Fluid Dyn.*, **19** (2005), 287–299. https://doi.org/10.1007/s00162-005-0167-3
9. A. V. Kuznetsov, The Onset of Thermo-Bioconvection in a Shallow Fluid Saturated Porous Layer Heated from Below in a Suspension of Oxytactic Microorganisms, *Eur. J. Mech. B/Fluids*, **25** (2006), 223–233. https://doi.org/10.1016/j.euromechflu.2005.06.003
10. A. V. Kuznetsov, Non-Oscillatory and Oscillatory Nanofluid Biothermal Convection in a Horizontal Layer of Finite Depth, *Eur. J Mech. B/ Fluids*, **30** (2011), 156–165. https://doi.org/10.1016/j.euromechflu.2010.10.007
11. A. V. Kuznetsov, Nanofluid Bioconvection in Water-Based Suspensions Containing Nanoparticles and Oxytactic microorganisms: Oscillatory instability, *Nanoscale Res. Lett.*, **6** (2011), 100. https://doi.org/10.1186/1556-276X-6-100
12. A. V. Kuznetsov, Bio-Thermal Convection Induced by Two Different Species of Microorganisms, *Int. Commun. Heat Mass*, **38** (2011), 548–553. https://doi.org/10.1016/j.icheatmasstransfer.2011.02.006
13. S. Nadeem, S. Saleem, Analytical treatment of unsteady mixed convection MHD flow on a rotating cone in a rotating frame, *J. Taiwan Inst., Chem. Eng.*, **44** (2013), 596–604. https://doi.org/10.1016/j.jtice.2013.01.007

14. L. Tham, R. Nazar, I. Pop, Steady mixed convection flow on a horizontal circular cylinder embedded in a porous medium filled by a nano fluid containing gyro tactic micro-organisms, *J. Heat Transfer.*, **135** (2013), 102601. https://doi.org/10.1115/1.4024387
15. K. Zaimi, A. Ishak, I. Pop, Stagnation point flow toward a stretching/shrinking sheet in a nanofluid containing both nano particles and gyrotactic micro-organisms, *J. Heat Transfer.*, **136** (2014), 041705. https://doi.org/10.1115/1.4026011
16. C. S. K. Raju, N. Sandeep, Dual solutions for unsteady heat and mass transfer in Bio-convection flow towards a rotating cone/plate in a rotating fluid, *Int. J. Eng. Res. Afr.*, **20** (2016), 161–176. https://doi.org/10.4028/www.scientific.net/JERA.20.161
17. W. J. Minkowycx, P. Cheng, Free convection about a vertical cylinder embedded in a porous medium, *Int. J. Heat Mass*, **19** (1976), 805–813. https://doi.org/10.1016/0017-9310(76)90135-6
18. P. Cheng, W. J. Minkowycz, Free convection about a vertical flat plate embedded in a porous medium with application to heat transfer from a dike, *J. Geophys. Res*, **82** (1977), 2040–2044. https://doi.org/10.1029/JB082i014p02040
19. M. Kumari, I. Pop, G. Nath, Finite-difference and improved perturbation solutions for free convection on a vertical cylinder embedded in a saturated porous medium, *Int. J. Heat Mass*, **28** (1985), 2171–2174. https://doi.org/10.1016/0017-9310(85)90112-7
20. J. H. Merkin, Free convection from a vertical cylinder embedded in a saturated porous medium, *Acta Mechanica*, **62** (1986), 19–28. https://doi.org/10.1007/bf01175850
21. J. H. Merkin, I. Pop, Mixed convection boundarylayer on a vertical cylinder embedded in a saturated porous medium, *Acta Mechanica*, **66** (1987), 251–262. https://doi.org/10.1007/BF01184297
22. F. C. Lai, I. Pop, F. A. Kulacki, Free and mixed convection from slender bodies of revolution in porous media, *Int. J. Heat Mass*, **33** (1990), 1767–1769.
23. F. C. Lai, C. Y. Choi, F. A. Kulacki, Coupled heat and mass transfer by natural convection from slender bodies of revolution in porous media, *Int. Commun. Heat Mass*, **17** (1990), 609–620. https://doi.org/10.1016/0735-1933(90)90009-9
24. S. M. Hussain, M. K. Mishra, I. Alraddadi, I. A. Al-Luhaybi, Thermal analysis of trihybrid (Co+ ZrO2+ Au/H2O) nanofluid flow through the exponentially deformable surface with Lorentz force and Navier's slippage constraint, *Int. J. Numer. Method. H.*, **35** (2025), 1680–1712. https://doi.org/10.1108/HFF-03-2025-0140
25. I. Alraddadi, S. M. Hussain, A. G. Almutairi, M. K. Mishra, Implications of slippage constraint and aligned Lorentz force on the ternary hybrid nanofluid flow over an exponentially deformable surface, *Multiscale and Multidiscip. Model. Exp. and Des.*, **8** (2025), 269. https://doi.org/10.1007/s41939-025-00864-6
26. S. M. Mabrouk, E. H. Nasr, A. E. Kabeel, A. S. Rashed, Enhanced Bioconvection Adjacent to Permeable Cylinder in Hybrid Nanofluids: Bacteria Distribution and Physical Features under Magnetic Field Influence, *J. Eng. Phys. Thermophy.*, **98** (2025), 454–467. https://doi.org/10.1007/s10891-025-03119-w
27. A. S. Rashed, E. Nasr, S. M. Mabrouk, Bioconvective Flow Surrounding a Thin Surgical Needle in Blood Incorporating Ternary Hybrid Nanoparticles, *Comput. Methods Differe.*, 2024.
28. M. Sohail, E. R. El-Zahar, A. A. A. Mousa, S. Althobaiti, N. A. Shah, J. D. Chung, Finite element analysis for ternary hybrid nanoparticles on thermal enhancement in pseudo-plastic liquid through porous stretching sheet, *Sci. Rep.*, **12** (2022), 9219. https://doi.org/10.1038/s41598-022-12857-3

29. G. K. Ramesh, J. K. Madhukesh, R. Das, N. A. Shah, S. J. Yook, Thermodynamic activity of a ternary nanofluid flow passing through a permeable slipped surface with heat source and sink, *Waves Random Complex*, **35** (2022), 3499–3519. https://doi.org/10.1080/17455030.2022.2053237
30. A. Rauf, Faisal, N. A. Shah, T. Botmart, Hall current and morphological effects on MHD micropolar non-Newtonian trihybrid nanofluid flow between two parallel surfaces, *Sci Rep*, **12** (2022), 16608. https://doi.org/10.1038/s41598-022-19625-3
31. C. S. K. Raju, S. Saleem, S. U. Mamatha, I, Hussain. Heat and mass transport phenomena of radiated slender body of three revolutions with saturated porous: Buongiorno's model. *Int. J. Therm. Sci.*, **132** (2018), 309–315. https://doi.org/10.1016/j.ijthermalsci.2018.06.016
32. M. D. Kumar, C. S. K. Raju, H. Ashraf, N. A. Shah, A. Ali, A. Mennouni, et al., Analysis of dynamical assisting and opposing flow characteristics of darcy surface-filled ternary nanoparticles and Fourier flux: Artificial neural network and levenberg method, *J. Circuit., Syst. Comp.*, **33** (2024), 2440001. https://doi.org/10.1142/S0218126624400012
33. B. Manvi, J. Tawade, M. Biradar, S. Noeiaghdam, U. F. Gamiz, V. Govindan, The effects of MHD radiating and non-uniform heat source/sink with heating on the momentum and heat transfer of Eyring-Powell fluid over a stretching, *Results Eng.,* **14** (2022), 100435. https://doi.org/10.1016/j.rineng.2022.100435
34. S. M. Hussain, M. R. Mishra, G. S. Seth, A. J. Chamkha, Dynamics of heat absorbing and radiative hydromagnetic nanofluids through a stretching surface with chemical reaction and viscous dissipation, In: *Proceedings of the Institution of Mechanical Engineers*, *Part E: Journal of Process Mechanical Engineering*, **238** (2022), 101–111. https://doi.org/10.1177/095440892210961
35. F. C. Lai, C. Y. Choi, F. A. Kulacki, Coupled heat and mass transfer by natural convection from slender bodies of revolution in porous media, *Int. Commun. Heat Mass*, **17** (1990), 609–620. https://doi.org/10.1016/0735-1933(90)90009-9

AIMS Press

© 2025 the Author(s), licensee AIMS Press. This is an open access article distributed under the terms of the Creative Commons Attribution License (http://creativecommons.org/licenses/by/4.0)